HOST UNIVERSITY: Ghent University

FACULTY: Faculty of Engineering and Architecture

DEPARTMENT: Department of Structural Engineering and Building Materials

Academic Year 2022-2023

Numerical Modelling of Water Spray Impingement Cooling
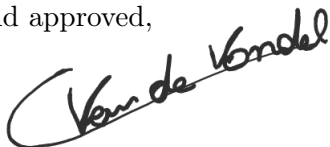
Cédric Van de Vondel

Supervisor: Prof. Dr. Tarek Beji

Master thesis submitted in the Erasmus+ Study Programme

International Master of Science in Fire Safety Engineering

DISCLAIMER

Read and approved,

Cédric Van de Vondel

10/05/2023

I

Acknowledgements

Abstract

The validation study done in this paper on the capabilities of FDS, to replicate an experiment in water cooling of a hot steel plate, has resulted in concluding that this particular CFD program is capable of producing relatively accurate results and having thus a good agreement with the experimental data. The experiment consisted of a hot metallic steel plate that was heated up, using a radiative panel, to 600 °C and then cooled with a water spray to ambient temperatures. The heating and cooling output data of the simulations are agreeing to those achieved in the similar experiments. Crucial factors for achieving these decent results were mainly the mesh size and its set-up regarding the objects implemented into the simulation, the high enough heat transfer coefficient, the correct specific heat of steel and the inclusion of water inside the steel plate. The default heat transfer coefficient between the water droplets and the hot plate for example proved to be much lower than the coefficient of the experiment and thus also much lower than the one used in the simulations to achieve the best agreeing results. The specific heat of steel used in the simulations is a very determining parameter when it comes to the heating phase of the steel plate.

Keywords— Validation study, FDS, Fire Dynamics Simulator, Surface wetting, Water spray, Boiling curve, Weber number, Coverage area

Extended Abstract

Introduction

The subject of this dissertation is on **Numerical Modelling of Water Spray Impingement Cooling**. The thesis paper presents a validation study of the Computational Fluid Dynamics (CFD) modelling capabilities on the interaction of water sprays with non-flaming surfaces.

Experimental Set-Up

The validation study, done in Fire Dynamics Simulator or FDS version 6.7.7-intel-2021b, is based on well-documented and designed experiments found in a conference paper [1] presented at the 10th international Seminar on Fire and Explosion Hazards on monday the 23th of May.

FDS Set-Up

The overall goal is to replicate the experimental results. This is done by first relying on the default FDS 6.7.7 settings. And from those results, analysing if some particular parameters require modification or not. This was for example the case with the convective heat transfer coefficient between the impinging water and the hot steel plate. The paper is created in a step-wise approach. The first part consists of first simulating and examining the hot metallic plate. Secondly only the water spray system is reproduced in FDS 6.7.7 and analysed. To then merge both parts into a simulation combining the water spray with the hot metallic plate, like in the experiments. This final set-up in FDS version 6.7.7-intel-2021b can be seen in figure 1.

Results

For the **hot metallic plate** part, multiple heating up techniques in FDS 6.7.7-intel-2021b are discussed and analysed. The best option was found to be a constant net heat flux coming from the radiative panel. A sensitivity analysis regarding the mesh size and number of radiation angles is conducted to ensure decent results, resulting in a mesh size of 20 mm and 200 for the number of radiation angles. Later, water has been added to the steel plate to get a better agreement with the
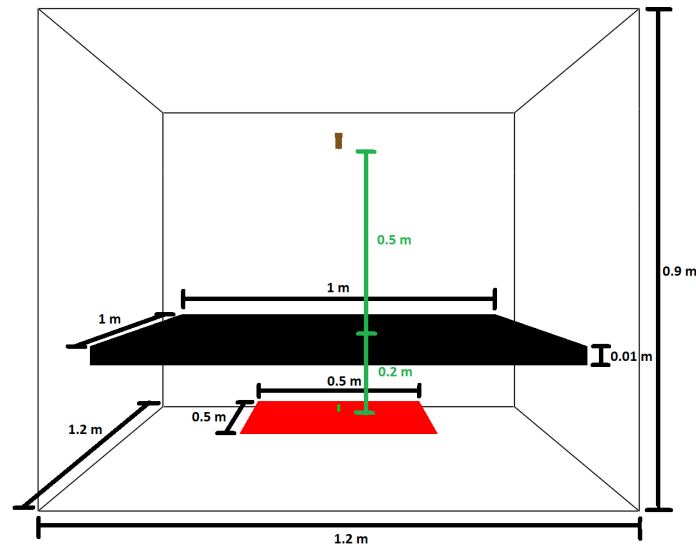
Figure 1: SmokeView setup of the experiment

experimental data. Here they measured a temperature plateau during the heating up phase of the metallic plate at around 100 °C for about 20 seconds. An analysis on the variation of conductivity and specific heat, over temperature, of the steel has been conducted to further validate these parameters in FDS version 6.7.7-intel-2021b.

The **water spray system** part consists of first finding the size and velocity distributions best resembling the experimental water spray data. This resulted in a volume-median diameter, initial droplet velocity out the nozzle and a width of the Rosin-Rammler distribution of respectively 188 µm, 70 m/s and 3.3. Secondly repeating, for this set-up, the sensitivity analysis of the mesh size but also the number of particles per second injected into the computational domain. Again concluding that a 20 mm mesh size is sufficient and that a value of 5000 for the number of particles per second yields decent results for this validation study.

After **combining the previous parts** into one simulation. The temperatures, velocities, heat fluxes and more are analysed. An important factor here to achieve a good agreement with the experiments is changing the heat transfer coefficient from the default value of 300 W/(m².K) to a much higher value like 50 000 W/(m².K). A fairly similar cooling rate compared to the experiments is achieved. The experiments managed to reach ambient temperature at the top side of the steel plate in approximately 4 seconds after water spray activation, in FDS version 6.7.7 this was achieved after 5.3 seconds. The temperature evolution can be seen in figure 2. The dynamic model, where the heat transfer coefficient changes with temperature, was also simulated and resulted in even faster cooling rates. For this set-up we reached ambient temperature in only 2.4 seconds. The difference of Mono- vs Poly-disperse during simulations told us that the Poly-disperse simulation is 12% more accurate in this set-up case, compared to the Mono-disperse method, but also requires 12% more computational time. The simulated coverage area of the water spray compared to those predicted in
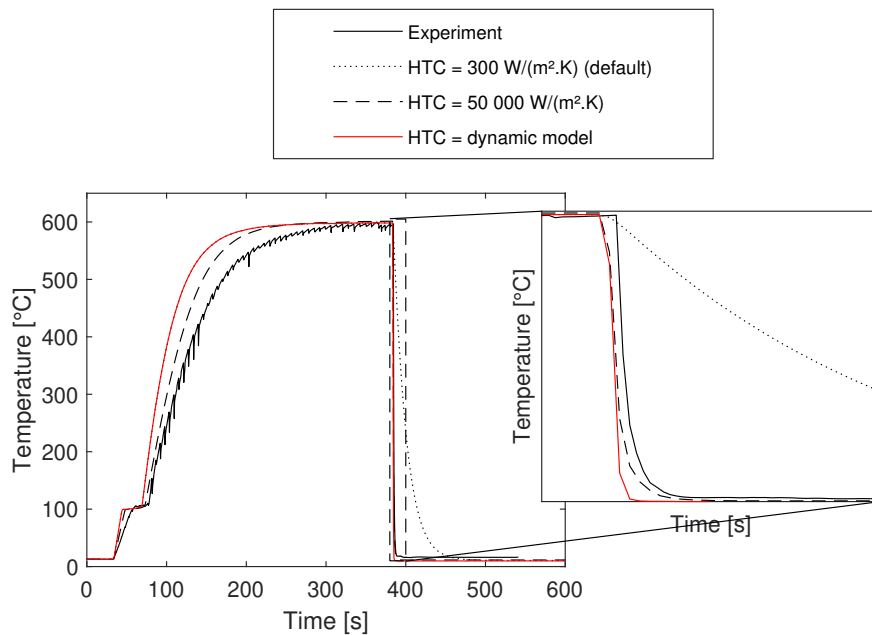
Figure 2: Temperature evolution

reality are, after making some assumptions, reasonably agreeing with each other. This is analysed by using the droplet diameter, downwards droplet velocity and particle mass flux Z measurements over different radial distances from the center of the steel plate. The boiling curve received from the experiments differs from the boiling curve replicated with the output data of FDS 6.7.7 due to some known limitations of the simulations. Likewise is the Weber number found to be slightly smaller with FDS 6.7.7 due to again some known limitations of our simulations.

Conclusion

The conclusion of this paper is that FDS version 6.7.7-intel-2021b is capable of delivering decent results while still using a fairly simple input file but where a few crucial FDS 6.7.7 settings, like the heat transfer coefficient between the water droplets and the hot plate, require modification.

References

[1] Acem Z., Mehaddi R., Dréan V., Laumesfeld J., Parent G., Collin A., Proal N., and Wilhelm A. "Water sprays cooling of a hot metallic plate", 10th international Seminar on Fire and Explosion Hazards, 10th may at 11:10.

Contents

List of Figures

List of Tables

Nomenclature

Acronyms

CFD	Computational Fluid Dynamics	
CNF	Cumulative Number Fraction	
CPU	Computational time	
CVF	Cumulative Volume Fraction	
FDS	Fire Dynamics Simulator	
HPC	High Performance Computing	
HRR	Heat Release Rate	
HTC	Heat transfer coefficient	$[W/(m^2.K)]$
IOR	Index of Orientation	
LES	Large Eddy Simulation	
MS	Measurements	
NFD	Number Fraction Distribution	
PDF	Probability Density Function	
PDPA	Phase Doppler Particle Analysis	
RA	Number of radiation angles	
RTE	Radiation Transport Equation	
SMD	Sauter mean diameter	$[\mu m]$
VFD	Volume Fraction Distribution	

Dimensionless Numbers

Ma	Mach number
Nu	Nusselt number
Pr	Prandtl number
Re	Reynolds number

Greek Symbols

δ	Droplet diameter	[m]
ϵ	Emissivity	[-]
γ	Rosin-Rammler distribution width parameter	[-]
ρ	Density	[kg/m^3]
σ	Log-normal distribution width parameter	[-]
σ	Stefan-Boltzmann constant	[5.67.10^{-8} J/(s.m^2.K^4)]

Latin Characters

ΔE	Internal energy	[kJ/kg]
ΔT_s	Excess surface Temperature	[°C]
$\dot{Q}$	Heat release rate	[kW]
$\dot{q}''$	Heat flux	[kW/m^2]
$\dot{V}$	Flow rate	[l/min]
c	Specific heat	[kJ/(kg.K)]
D_d	Droplet diameter	[m]
D_{v50}	Volume-median diameter	[m]
e	Thickness	[m]
F_v	Cumulative volume fraction	[-]
h	Convective heat transfer coefficient	[W/(m^2.K)]
k	Thermal conductivity	[W/(m.K)]
M	Molecular weight	[g/mol]

N_p	Number of particles per second	[particles/s]
p	Pressure	[bar]
Q	Energy	[kJ]
T	Temperature	[°C]
t	Time	[s]
u	Particle velocity	[m/s]
We	Weber number	[-]

Other Symbols

δx	Mesh cell size in FDS	[m]

Superscripts

'	derivative

Subscripts

c	Convective
r	Radiative
sat	Saturated
sim	Simulation
s	Surface

Chapter 1

Introduction

In the introduction we will go over the references of relevant recent literature found on the subject of this thesis. It is important to understand the way FDS works and what kind of methods it uses as well as the data we review it against.

1.1 Background

Extinguishing fires with liquid water has been a big part of fire suppression since a very long time. Water is an economically affordable and very effective way to cool down a heated object. This is caused by the high heat dissipation and efficient way of heat removal from either the flame, the hot products of combustion or from very hot surfaces. The latter is the main focus point in this thesis, cooling the surface of combustible items and in doing so preventing pyrolysis.

Pyrolysis is the chemical decomposition of a material into volatile products that can result under appropriate conditions, reaction with oxygen and the release of heat, into a flame. The surface temperature required here is typically very high because this pyrolysis demands a high amount of energy. As mentioned above, the water can be used for cooling this surface temperature enough to prevent pyrolysis. Another way of cooling via water droplets out of a spray is that water also has the ability to absorb radiant heat. Experiments have been done, see [1], with different types of hydraulic nozzles and different operating water flows, giving the following conclusions. The attenuation of the thermal radiation can be increased by increasing the flow through the nozzle or by decreasing the droplet diameter. A nozzle characterised by a high flow rate, large droplet size and high velocity resulted in the most effective nozzle with the highest attenuation. A nozzle with a low flow rate, small droplets and low velocity gave the most efficient nozzle with the highest absorption of radiant heat per unit flow.

An extensive literature review on spray cooling of solid fuel surfaces was already done by Grand et al. [2] and Yin et al. [3]. Four distinct boiling heat transfer regimes were identified by Bejan [4] for water at atmospheric pressure and depending on the temperature the heated solid surface

possesses. From lower to higher excess surface temperature there is: natural convection boiling, nucleate boiling, transition boiling and film boiling (1.1).
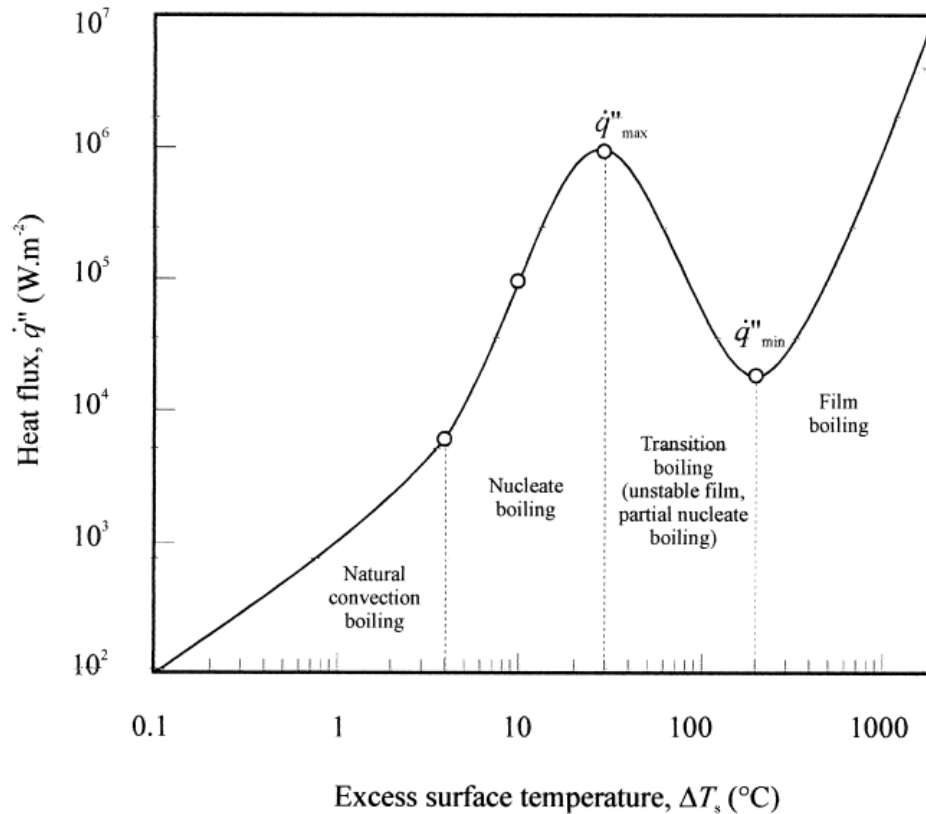
Figure 1.1: The four regimes of pool boiling in water at atmospheric pressure, figure taken from [2]

The excess surface temperature or ΔT_s is calculated by deducting the surface temperature by the saturated temperature (T_{sat}) of liquid . The natural convection boiling regime where the heat flux is small and increases slowly with surface temperature, has hardly any phase change in the liquid film. With increasing the surface temperature, spray cooling enters the nuclear boiling regime. Here the cooling performance is significantly improved, as can be seen by the steep slope of the boiling curve. If the surface temperature increases even further to a specific critical value, indicated by $\dot{q}''_{max}$ on figure 1.1, localized vapor blankets will take the place of the bubble nucleation. The peak of the surface heat flux or Critical Heat Flux (C.H.F.) is then reached and will no longer increase due to the complete blanketing of the surface by water vapor.

The high surface temperatures of the solid surfaces put most of fire safety application with water spray in the film boiling regime (above 200°C-300°C). The film boiling is a continuous film of water vapour that is formed between the liquid water droplets and the hot solid surface. See the liquid film for low droplet velocity and high surface temperature in figure 1.2a and see the film boiling regime in figure 1.2b. The plate is isolated from the water by the film vapour, which results in

relatively low heat exchange. When the temperature of the solid surface (T_s) decreases, the heat flux also goes gradually down until reaching a certain point, on figure 1.1 defined as $\dot{q}''_{min}$. This is the minimum heat flux leaving the surface and the temperature corresponding with this heat flux is named the Leidenfrost temperature. Going to even lower surface temperatures will cause the vapour film, mentioned before, to collapse and resulting in a sudden increase of heat flux. This Leidenfrost temperature is estimated by Bejan [4] to occur between T_s = 30°C and 200°C for water at atmospheric pressure and part of the transition boiling regime.

(a) Liquid droplets - surface interaction, [5]   (b) Liquid film - surface interaction, [3]
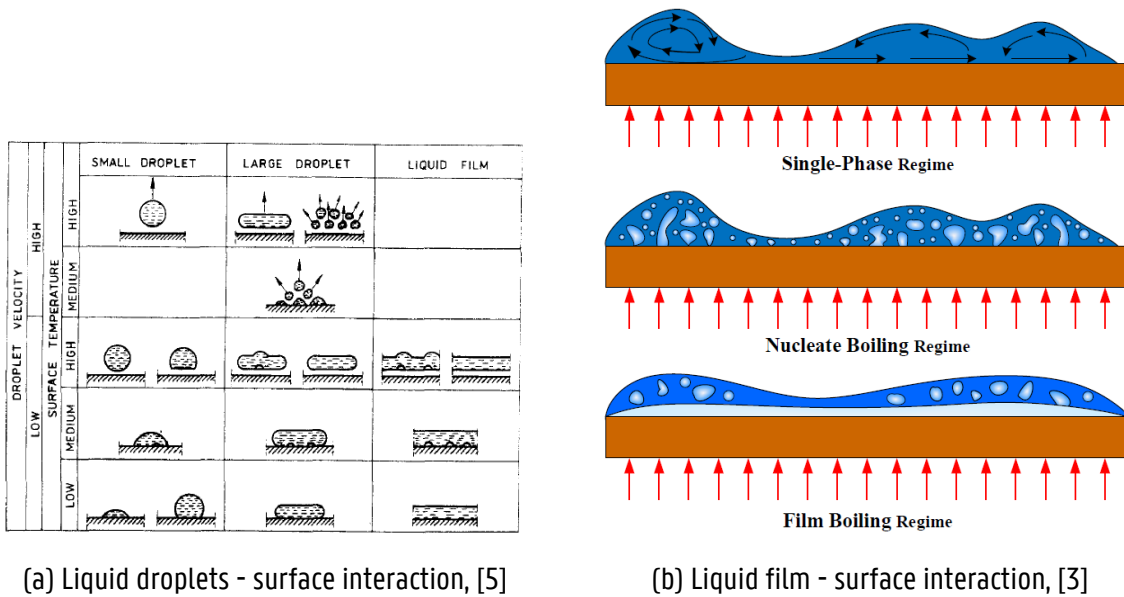
Figure 1.2: Detailed states of liquid droplets/film - surface interaction

Ito et al. [6] uses a non-dimensional Weber number that characterizes the behaviour of spray droplets impinging onto horizontal heated surfaces. This Weber number is the ratio of the inertial force to the surface tension force and can be defined as follows:

$$We = u^2 \rho D_d / \sigma \qquad (1.1)$$

ρ is the density of water, u is the velocity of the droplets, D_d is the droplet diameter and σ is defined as the surface tension of water. This Weber number is used in the experimental paper of Acem et al. [7]. This number can also be based on the Sauter diameter and mean velocity as done by Acem et al and is calculated to be 80 or higher in the experimental paper. Ito et al. [6] indicate that for $We \geq 80$, the striking droplets after impact form a thin, unfolded liquid film, which then breaks up into smaller droplets. According to Rymkiewicz et al. [5] there are three main parameters when defining the evaporation of a droplet on a surface: the droplet impact velocity, the initial surface temperature and the droplet size. These three parameters will also be discussed in length when

creating the FDS file later in the thesis.

In the experimental work done by Labergue et al. [8] for cooling a hot surface using full poly disperse cone sprays, the goal was to link the spray properties to the heat removed from the heated surface. The conclusion presented is that the cooling efficiency decreases with a decrease of water mass flux through the nozzle. This is also causing an increase of the Leidenfrost temperature. Increasing the vertical velocity of the droplets at impact would result in a lower heat flux.

An import factor for analysing and researching a water spray in reality is particle characterization. This can be done by using a laser-based phase Doppler particle analyzer or PDPA [9]. The analyzer can measure for example the size of droplets and at what speed they are moving by the following method. When moving through a sampling volume, the particles will pass light and dark fringes. A fringe pattern, which is a series of light and dark fringes, is the result of the intersection of two laser beams. When crossing a light fringe it will scatter this light and some of the scattered light will reach an optical receiver. When crossing the dark fringes no light will be scattered. And by then knowing the frequency at which the light fringes are received, information about the velocity of the particle can be collected. This can be done by the use of only one light detector. A second is needed to measure the spatial frequency of the scattered fringes. The spatial frequency is the spacing that exist between the scattered fringes at the light collecting optics and is measured as a phase shift between two electrical signals. These signals are the result of the scattered light. This can than lead to information regarding the size of the particles. A way for making more trustworthy data is by implementing redundancy. This can be easily done by using three photo detectors so two independent measurements for the size of the droplets are possible.

1.2   Experimental data

The experimental data used in this thesis report was achieved by the team of Acem, Mehaddi, Dréan, Laumesfeld, Parent, Collin, Proal and Wilhelm [7]. The team provided extra data, not available in the paper cited, to better analyse the results later. When the experiment or experimental data is stated in this thesis, this is the paper we refer to.

Their paper covers multiple experiments of water cooling spray systems on a hot steel plate. In the experiment, they used three different nozzles and assessed the cooling efficiency. The surface temperatures measured during their work were a result of using K-type thermocouple wires, which they directly welded on the steel plate in a separated contact. When looking at the water spray, the droplets size (Sauter Mean diameter, range: 170-230 µm) and velocity (Mean velocity, range: 5.6-22.4 ms^{-1}) were recorded during the tests. Also the overall size and velocity distribution were measured. After the steel plate has reached a surface temperature of 600 °C, the cooling system is manually activated. When the activation of the spray occurs, the heating mechanism, radiative panel, is stopped. The authors observed that the cooling rate of the experiment was very high

with a cooling period between 4 seconds and 1 minute to reach ambient temperature (20°C) again, this was mainly dependent on the type of spray nozzle used. They also observed that the film boiling regime, mentioned before, was never achieved in their experiments. They made the case that the high velocity of the droplets reaching the hot metallic plate causes the droplets to go through and break up the vapour film that isolates the plate from the water. So when the cooling occurs, it immediately starts in the transition boiling regime. When the cooling continues, the heat flux increases until reaching CHF or Critical Heat Flux of around 2.76 MW/m².

1.3 Fire Dynamics Simulator

Like mentioned before, the goal is to try and replicate this experiment as well as possible and compare the results. The key words here are "as well as possible". There is almost always a limit to the possibilities in simulation. May this be the computational time, required information, mesh size, amount of droplets simulated or something else. It is the responsibility of the creator of a simulation to resemble the reality as best as possible, with also mentioning the limits and assumptions used during the creation of the simulation.

Computational Fluid Dynamics is a numerical tool that solves governing equations that are used to describe fluid flow, i.e., the Navier-Stokes equations, the continuity equations, and all additional conservation equations, e.g., the energy or species concentrations.

One of the most used Computational Fluid Dynamics (CFD) codes for fire scenarios is the Fire Dynamics Simulator (FDS). FDS is a large-eddy simulation (LES) code for low-speed flows, with an emphasis on smoke and heat transport from fires. It also consists of a SmokeView part, a separate visualisation program that is used to display the results of an FDS simulation. For the validation of CFD codes such as the Fire Dynamics Simulator, experimental data is used. In this paper, the aim is to validate the models used in the simulations during the heat transfer between water spray droplets and a hot metallic plate. The results provided here are a continuation of work carried out previously [10].

The Fire Dynamics Simulator, **version 6.7.7-intel-2021b**, is used in this paper. The simulation ran on the HPC (High-Performance-Computing) facilities of UGent. The Fire Dynamics Simulator solves numerically a form of the Navier-Stokes equations and is mainly appropriate for Low-speed flows (Ma <0.3), thermally-driven flows and emphasis on smoke and heat transport from fires [11]. The partial derivatives of conservation equations of mass, energy and momentum are approximated as finite differences. The solution is updated over time in a three dimensional rectilinear grid. Large Eddy Simulation is used to model the turbulence. Radiative heat transfer is included in the model by solving the radiative transfer equation for a grey gas or, for some limited cases, by a wide band model.

Chapter 2

Experimental Set-Up

The set-up of the experiment made, 2.1, by Acem Zoubir et. [7] will be presented in the following sections.

2.1 Hot Metallic plate

The heating of the steel plate is done by using a radiative panel. The steel plate itself is one square meter with a depth of 2 mm (1m x 1m x 0.002 m). The plate is coated with resistant black paint. The radiative panel is a bit smaller, having a size of 0.5m x 0.5m, and propane fueled. The distance between the steel plate and the radiative panel is 20 cm. The radiative panel delivers a total power of 50 kW, where half is estimated to be radiative, giving us a radiative heat flux of 100 kW/m². Flux measuring devices were installed at the center of the black steel plate giving a total heat flux of 88 kW/m², radiative heat flux of 54 kW/m² and a convective heat flux of 24 kW/m².

The experiment was conducted in two different setups, a horizontal setup and a vertical one. But for this thesis we remain focused on the horizontal configuration.

2.2 Water spray

Another important part of the set-up is the water spray. In the paper they mention three different nozzle types used during the experiment, listed below.

- Protectospray D3 nozzle from Tyco

- Assembly of four flat jet nozzles TPU400067 from Spraying Systems

- SU42 conical jet nozzle from Spraying Systems

We will focus during the simulations and in this paper on the last one, the SU42 nozzle. The SU42 is an air atomizing and air assisted nozzle producing a cone spray pattern with internal mix

impingement atomization forming very fine droplets. This twin-fluid water mist is regarded as a technique with a uniform cooling [12]. When consulting [13] a value of 19-22° is provided for the spray angle of this nozzle. The spray nozzle is put centered and at 50 cm above the heated steel plate.

Like mentioned in the introduction, the size and the (assumed vertical component of the) velocity of the droplets was measured at the height of the steel plate. This is done by using a SpraySpy device from AOM-systems or Advanced Optical Measurement systems. The SpraySpy has a sampling rate of around 250 MS/s [14]. The smallest droplet this device can measure is 1 μm, smaller than this will not be detected by the SpraySpy. There is also a limit in velocities of the droplets that can be measured, this cannot be higher than 100 m/s. The flow rate of the used water spray is 4.6 l/min, the water pressure is equal to 6.2 bar and the air pressure is 4.5 bar.

The water spray is activated when the heated steel plate reaches a quasi-steady state temperature. For the focused horizontal set-up with the SU42 this temperature is around 600°C. The theoretical coverage for this spray, according to the manufacturer [13], and at a distance of 50 cm is 18.5 cm. The theoretical coverage is calculated from the spray angle and the distance from the nozzle orifice. This value is based on the assumption that the angle of the spray is constant throughout the entire spray distance. In reality this spray angle will not hold for long spray distances, meaning a smaller spray coverage is expected in reality.

Figure 2.1: Setup of experiment from Acem et. [7]

Chapter 3

FDS Set-Up

As described in the following part of the thesis, a series of simulations were performed to evaluate the performance of FDS 6.7.7 2021b in capturing the rather complex interaction between the hot steel plate and the water droplets. For better usage and understanding of the Fire Dynamics Simulator, FDS guides were used [15].

The approaching water droplets interact with the hot air above the heated steel plate before coming into contact with the plate itself. The interaction with the rising plume affects the impact velocity, the size distribution at the plate surface, the velocity distribution and the approaching temperatures of the droplets. The step-wise approach used, divides the simulations process into 3 parts:

- Simulating the hot steel plate and radiative panel below.

- Simulating the water spray system.

- Simulating the combination of the water spray system and the hot metallic plate heated by the radiative panel.

The overall setup of the simulation in SmokeView can be seen in figure 3.1.

3.1   Hot Metallic plate

This part focuses on the heating of the 1 m² steel plate and achieving, as main goal, the required temperature similar to the experiments.

The file always consist of a time period for the simulation to achieve what needs to be achieved. 600 seconds was put here for the simulation to run its full course. The experimental data and curves, especially the start of heating, may differ from later in the thesis. This is because the experimental data in this section is changed so that the heating of the plate starts at 0 seconds to compare more easily with the simulation results. The setup starts in ambient conditions at a temperature
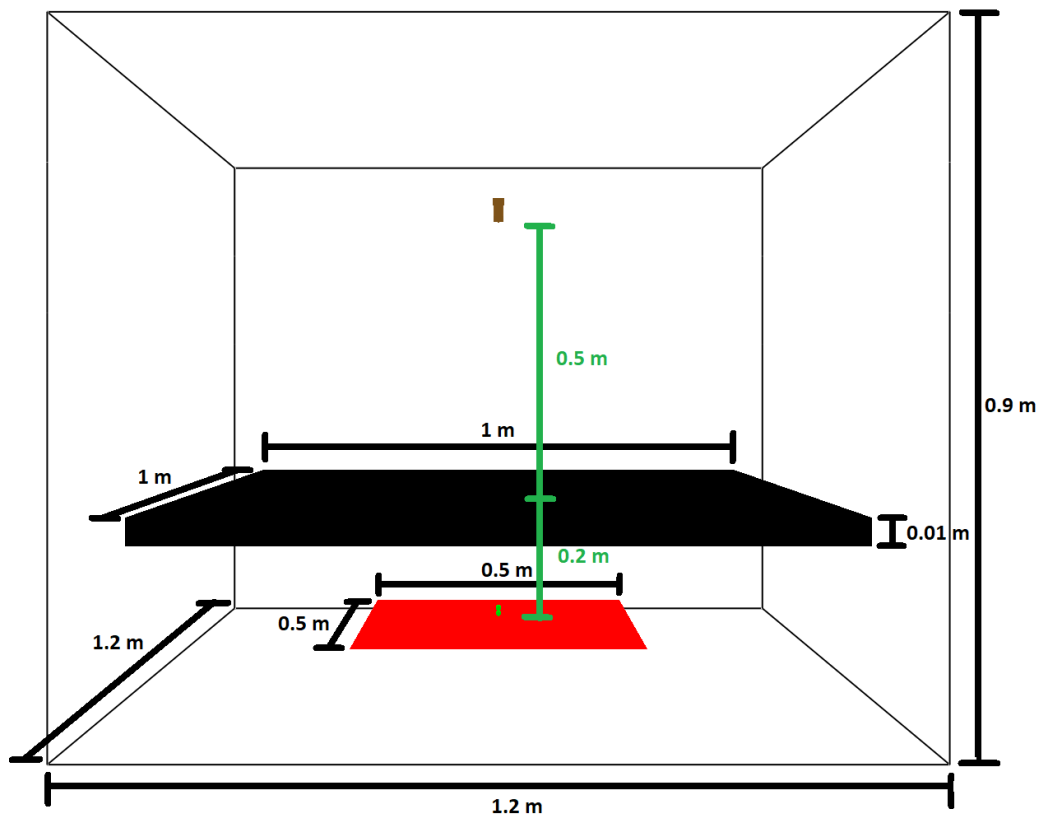
Figure 3.1: SmokeView setup of the experiment

of 12.75°C, a few seconds later we have the heating up of the steel plate until steady temperatures were reached over a long enough period of time.

When defining a material in FDS, MATL_ID, some key properties need to be included. For the steel, the conductivity used was 45.8 W/m.K, the specific heat used was 0.460 kJ/kg.K and the density used was 7850 kg/m³, values were found in "An Introduction to Fire Dynamics" [16].

Extra inputs were added to the FDS file like slice files, devices and boundary conditions. To be able to analyse the results various quantities need to be recorded during the simulation. Therefore, some devices (DEVC) and boundary slice files (BNDF) were added. The devices that simulate the thermocouples used in the experiments are put at the same location. This solid phase output device to the solid surface uses WALL_TEMPERATURE to measure the temperature over time. The devices also have a given orientation defined by IOR.

Another important part is defining that the mesh boundary condition is open at all sides. In doing so, simulating in what resembles as an open area where no direct walls or other obstacles play any part in the FDS calculations. This is done by defining an open boundary or VENT to all the 6 faces of the computational domain (XMIN, XMAX, YMIN, ...).

3.1.1 Heating up to required temperature

To achieve the goal of heating the steel plate to a temperature of around 600 °C, multiple methods were considered. The first one is simulating only the steel plate itself, without using a radiative panel to heat up the plate but using other options to reach the required 600°C. The second and most desired method was simulating both the steel plate and the radiative panel. This way the experiment is more accurately simulated using the same set-up as given in the paper by Acem Zoubir et. [7]. It is important to also note that in FDS, a positive heat flux means that the wall or obstacle is heating up the surrounding gases. When defining or finding a negative heat flux the opposite is true and the wall or obstacle would cool the surrounding gases.

Multiple options are able to achieve this primary goal, listed below.

By using the **steel plate methods** a simulation of the steel plate is made without using a radiative panel. The first option here is specifying a solid surface temperature to the steel plate (1a). Another option is specifying a net heat flux in kW/m² (1b). When specified, FDS calculates the surface temperature required to ensure that the combined radiative and convective heat flux from the surface is equal to the NET_HEAT_FLUX. A third option requires the programmer to insert a specific CONVEC-TIVE_HEAT_FLUX in kW/m². This option is discarded because this method relies on the EMISSIVITY, for which we don't know the exact value. A fourth option that was considered was using an IN-TERNAL_HEAT_SOURCE in kW/m³ (1c). And a fifth and final choice is working with an external flux (1d), and using this to heat up the steel plate to a value of 600 °C. This final external flux option was used by Thushadh Wijesekere in his paper of numerical modelling of water spray impingement cooling [10].

The **radiative panel methods**, where we use the simulated radiative panel, can use some of the same options as mentioned above.

1. **Steel plate methods**

    (a) TMP_FRONT = 600°C

    (b) NET_HEAT_FLUX = 36 kW/m²

    (c) INTERNAL_HEAT_SOURCE = 35000 kW/m³

    (d) EXTERNAL_FLUX = 36 kW/m²

2. **Radiative panel methods**

    (a) TMP_FRONT = 950°C

    (b) NET_HEAT_FLUX = 112 kW/m² (Used option)

The numbers for heat fluxes and temperatures above were found by first implementing the values found from the experiment (2.1) and then, with trial and error, finding the best values for each

method to give a steady 600 °C to the cool or top side of the steel plate over a long enough period of time. The internal heat source, 1c, was first estimated to be 44 000 kw/m³ by calculating the volume of the steel plate (1 m² . 0.002 m = 0.002 m³) and then dividing the 88 kW found in Acem paper [7] by this volume. The first estimation for the net and external heat flux, 1d and 1b, of the steel plate was 88 kW/m². The 950 °C temperature for the radiative panel method, 2a, was found by first simulating the net heat flux method 2b and then observing the temperature of radiative panel to get an estimation. The last and used method with the net heat flux, 2b, was found by starting with a value of 200 kW/m² and adjusting this value until reaching steady 600 °C at the steel plate.

The heat conduction losses to the bottom side of the radiative heat panel were set to zero by setting BACKING='INSULATED' at the FDS file.

3.1.2   Sensitivity mesh size analysis

When doing a simulation, the mesh size is very important. A mesh size that is too large can lead to unrealistic data results or a mesh size too small can lead to very long computational times. To make the right decision on how big the cell size needs to be in the simulation, a sensitivity analysis is done. Four different mesh cell sizes were compared, δx (mm) = 10 mm, 20 mm, 40 mm and 50 mm.

3.1.3   Sensitivity radiation angles analysis

Another important sensitive parameter in creating a CFD simulation like this is the amount of radiation angles or RA used. This is one of the ways to improve the spatial and temporal accuracy of the discrete radiation transport equation (RTE). The default number of angles in FDS is 100. Increasing this number would, at most cases, also increase the computational time, an analysis needs to be done to determine if the increase in computational time is worth the more accurate results. For this reason we increase and decrease the NUMBER_RADIATION_ANGLES in the FDS file for a few simulations from 100 to 50, 200 and 400 angles. A way to analyse the required spatial resolution is with the use of slice (SLCF) files or in this case boundary (BNDF) files. The ideal thing to see is a smooth and circular pattern far from the heat source, but because of the finite number of solid angles during the simulation, you can see in the far field a star-like pattern. This can be solved by increasing the number of angles until you see a smooth pattern over the total region of the simulation.

Two values that are not altered in the FDS file are the TIME_STEP_INCREMENT, that has a default value of 3 and the ANGLE_INCREMENT, having a default value of 5. The TIME_STEP_INCREMENT refers to the frequency of calls to the radiation solver over a given time step. ANGLE_INCREMENT on the other hand is the increment over which the angles are updated. Using the default values gives us an updated radiation transport equation every 15 time steps. This is enough in this simulation because increasing this frequency will greatly increase the computational time with it and stated in the FDS

user guide it rarely adds accuracy to the overall calculation of the radiation solver. Spatial resolution like mentioned above is far more important. Another value TIME_STEP_INCREMENT (default 1) is also not changed because no obvious delay in propagation of radiative intensity over multiple meshes is visual.

3.2   Water spray

The second section of this chapter will give further information on how the FDS file of the water spray system is set up. Parts of the file are already explained before like VENT or the starting temperature of 12.75 °C. And will not be repeated here.

3.2.1   Water spray properties

When using a water spray in FDS, the file requires a SPEC_ID and PART ID line. The SPEC_ID defines the gas species created by evaporation of the liquid droplets, in this case WATER VAPOR. By specifying a SPEC_ID, you are implicitly invoking the droplet evaporation model. The physical properties of WATER VAPOR are defined by FDS and can be found in [15] and [17].

The PART ID line includes the properties of the Lagrangian particles, in this case the liquid droplets. Later in the file the PART ID will be introduced into the calculation via the sprinkler of the water spray system on the PROP ID line. These properties contain the volume-median diameter or D_{v50} defined by the parameter DIAMETER (µm). This value plays a crucial part in setting up the water spray together with the width of the Rosin-Rammler distribution GAMMA_D and/or the width of the log-normal distribution SIGMA_D, but this will be explained in more detail in 3.2.2. The CHECK_DISTRIBUTION on the part line can cause FDS to write out a cumulative distribution function for the water spray particle class. HEAT_TRANSFER_COEFFICIENT_SOLID was added to the PART ID after the default value of 300 W/(m².K) proved to be too low. This constant value defines the heat transfer coefficient between the solid steel plate and the liquid water droplets. Defining negative values, like -1, to this input parameter will result in turning on an empirical model that calculates the coefficient dynamically. Another parameter that was added to the PART ID line later was QUANTITIES. This way SmokeView is able to show interesting information regarding the particle diameter, temperature and velocity. The particle temperature here refers to the temperature of the particle itself rather than the local gas temperature or wall temperature that has been measured via other means, namely the devices and slice files.

The last part of the set-up in FDS is by defining the properties of the device or water spray used in the simulation. This consists of the FLOW_RATE in l/min, found in the experimental paper and is equal to 4.6 l/min. The OFFSET is the radius in meters of a sphere surrounding the sprinkler where the droplets are initially placed in the simulation and was given a value of 0.01 meter. The SPRAY_ANGLE is a pair of angles through which the droplets are sprayed and was not specified in

the paper but was like mentioned in the introduction of this thesis found in [13], namely 21°. As last we define a PARTICLE_VELOCITY which is the initial droplet velocity out of the spray, see more 3.2.3. These values are assumed because no exact data was found on the velocity at injection into the air. The device itself with ORIENTATION, time point when the spray is activated SETPOINT and location XYZ is all defined in the DEVC line. The location and orientation was at 50 cm high in the center of the mesh facing downwards. The time when the activation of the spray occurs is set at 400 seconds, giving the steel plate enough time to reach steady temperature of 600°C and corresponds roughly with the activation time of the spray in the experiments.

3.2.2 Size distribution

Like mentioned before, the size distribution plays a vital part in defining a water spray. We want this to have a good agreement with the original experiment data. This can be done in two different ways. The first one is the use of MONODISPERSE=.TRUE.. This means that all droplets created in the simulation will have the same diameter and there will not be any distribution regarding the droplet size. The other option is by defining a size distribution, like mentioned below using GAMMA_D and/or SIGMA_D. This DIAMETER is as mentioned before the volume median diameter. In this case the droplet diameter size is distributed so that 50 % of the spray volume has droplets with diameters smaller than this median value while the other 50 % has larger droplet diameters.

To understand what was required in the input of the water spray, DIAMETER and GAMMA_D we needed to look how FDS calculates the size distribution, citing [15] and [18].

In FDS there is the option of choosing between three size distributions: LOG-NORMAL', 'ROSIN-RAMMLER' and a combination of both 'ROSIN-RAMMLER-LOG-NORMAL'. The default version in FDS is the latter of the three. The size distribution is mostly represented in either the Rosin-Rammler or Rosin-Rammler-Log-normal form. The Rosin-Rammler-Log-normal uses the log-normal distribution function for smaller diameters ($D_d \leq D_{v50}$) and the Rosin-Rammler for larger ones ($D_d > D_{v50}$) as seen below, 3.1:

$$F_{v,D_d}(D_d) = \begin{cases} \frac{1}{\sigma\sqrt{2\pi}} \int_0^{D_d} \frac{1}{\delta} exp(-\frac{[ln(D_d)-ln(D_{v50})]^2}{2\sigma^2})\, d\delta & D_d \leq D_{v50} \\ 1 - exp[-ln(2)(\frac{D_d}{D_{v50}})^\gamma] & D_d > D_{v50} \end{cases} \tag{3.1}$$

where the width parameter of the log-normal part is related by 3.2 to the width of the Rosin-Rammler part.

$$\sigma = \frac{2}{\sqrt{2\pi}(ln(2))\gamma} \tag{3.2}$$

The mixed distribution is used in this thesis for achieving the best results. To work with this distribution two unknown parameters on the PART line are required, DIAMETER and GAMMA_D. A first estimation of these values is achieved by comparing the experimental Cumulative Volume Fraction graph with the inserted formula of the Rosin-Rammler-Log-normal in MATLAB R2021b, 5. Then trying to fit the generated graph to the experimental one by changing the values of the diameter and gamma until a good agreement was obtained. Then these found values were put in the FDS file as the initial size distribution values of the water spray, meaning at that this droplet size distribution will be present at the height of the nozzle itself. The results of the diameter histogram were then compared to the experimental diameter distribution. Because the experimental size distribution was measured at 50 cm below the nozzle spray, the values were adjusted again until also these histograms match the experimental data well.

3.2.3   Velocity distribution

The initial velocity, PARTICLE_VELOCITY, out of the SU42 nozzle is also an unknown parameter. This value is again found by comparing resulting PDPA velocity histograms of different initial velocity simulations with the experimental measurements.

3.2.4   Measuring devices: PDPA

Like in the hot metallic plate simulations, some devices were added to analyse the results. These devices simulate the Phase Doppler Particle Analysis (PDPA) measurements. This can provide information on the droplet velocity, size distribution and concentration. Especially the first two are relevant here because they can be used to directly compare the simulation results with the data from the experimental paper. The best way for this is by letting the PDPA output histograms with a set number of bins and limits. The values that are bigger or smaller than these limits will be added to the last or first bin of the histogram. This PDPA device is used to measure for example the diameter, downwards velocity and overall velocity of the droplets at 50 cm below the water spray, because this is the location where the hot steel plate will be located. During analysing and comparing of PDPA devices in FDS against experimental data, the measuring results of the device closest to the center of the metallic plate was used. For example D1-0 and v1-0, 5. A factor to keep in mind is that the PDPA devices cannot be put exactly at the location of the steel plate when we simulated the combined, hot steel plate and water spray, setup. This is because the obstacle would interfere with the measurements. So in the analyses of the combined simulation, the PDPA results are measured 1 cm above the steel plate. This will cause the results to have a small deviation from the exact measurements at 50 cm, and can be seen as a limitation of this simulation.

3.2.5   Sensitivity mesh size analysis

Like in the first part, a sensitivity analysis was required to make sure the mesh size is small enough to ensure decent results. The simulation was run with the following mesh sizes: 10 mm, 20 mm, 40 mm, 50 mm and 80 mm mesh cell size and used the default 5000 PARTICLES_PER_SECOND. They were evaluated on the size and velocity distributions the results yielded.   The computational time of the 10 mm mesh size was too large, CPU-time: 72 hours for 444.48 seconds of simulated time, so this mesh size was not considered for further analysis.

3.2.6   Sensitivity number of particles per second analysis

In FDS the parameter N_p or PARTICLES_PER_SECOND is used to define the number of particles per second for a water spray system. Because this can be a sensitive parameter a sensitivity analysis will also be conducted here, in order to prevent bad results or too long CPU times. According to [18], the computational time increases linearly with the N_p. Too low number of particles per second will on the other hand, cause the CPU time to increase in case of using the Rosin-Rammler distribution. The default value in FDS is 5000 particles/s. To find if the results are sensitive to this parameter we will do the 40 mm mesh simulation with 4 different N_p values (N_p = 5 000, 10 000, 50 000 and 100 000 s^{-1}).

3.3   Water spray system and heated plate

After simulating the metallic plate part and the water spray part as best as possible, a combined simulation of the entire setup is created.

To imitate the experiment as best as possible, the heating starts after 32.8 seconds into the simulation. After this there is the heating up phase of the steel plate until reaching quasi-steady state temperature of 600 °C. After 384.4 seconds the water spray is activated and the radiative panel is turned off.

3.4   List of simulations

As you can imagine, the amount of simulations done for this validation study is fairly high, around 170 in total. So to make a clear overview, a list is given below of the most important simulations and their input parameters. The first table, see 3.1, covers the simulations done for the hot metallic plate section of this paper. The second table, see 3.2, does the same but for the water spray simulations. And finally, the table 3.3 contains the combined simulations done for this thesis with the very last one, see black indication, being the final simulation and thus the simulation with the best agreement compared to the experiments.

Table 3.1: Hot metallic plate simulations

nr.	Mesh size (mm)	RA	Heating method	Water in steel present	k (W/(m.K))	c (kJ/(kg.K))	Group
1	10	100	Radiative panel: NET HEAT FLUX = 112 kW/m²	NO	45.8	0.46	Heating up phase
2	10	100	Steel plate: TMP FRONT = 600 °C	NO	45.8	0.46	
3	10	100	Steel plate: NET HEAT FLUX = 36 kW/m²	NO	45.8	0.46	
4	10	100	Steel plate: INTERNAL HEAT SOURCE = 35 000 kW/m³	NO	45.8	0.46	
5	10	100	Steel plate: EXTERNAL FLUX = 36 kW/m³	NO	45.8	0.46	
6	10	100	Radiative panel: TMP FRONT = 950 °C	NO	45.8	0.46	
7	10	100	Radiative panel: NET HEAT FLUX = 112 kW/m²	YES	45.8	0.46	Water added
8	10	100	Radiative panel: NET HEAT FLUX = 105 kW/m²	YES	45.8	0.46	
9	40	100	Radiative panel: NET HEAT FLUX = 105 kW/m²	YES	45.8	0.46	Constant k and c vs variation of k and c
10	40	100	Radiative panel: NET HEAT FLUX = 105 kW/m²	YES	4.3a	4.3b	
11	40	100	Radiative panel: NET HEAT FLUX = 105 kW/m²	YES	100	0.46	Different constant k and c values for steel
12	40	100	Radiative panel: NET HEAT FLUX = 105 kW/m²	YES	30	0.46	
13	40	100	Radiative panel: NET HEAT FLUX = 105 kW/m²	YES	45.8	0.8	
14	40	100	Radiative panel: NET HEAT FLUX = 105 kW/m²	YES	45.8	0.3	
15	10	100	Radiative panel: NET HEAT FLUX = 112 kW/m²	NO	45.8	0.46	Sensitivity mesh analysis
16	20	100	Radiative panel: NET HEAT FLUX = 112 kW/m²	NO	45.8	0.46	
17	40	100	Radiative panel: NET HEAT FLUX = 112 kW/m²	NO	45.8	0.46	
18	50	100	Radiative panel: NET HEAT FLUX = 112 kW/m²	NO	45.8	0.46	
19	20	50	Radiative panel: NET HEAT FLUX = 112 kW/m²	NO	45.8	0.46	Sensitivity analysis on the number of radiation angles
20	20	200	Radiative panel: NET HEAT FLUX = 112 kW/m²	NO	45.8	0.46	
21	20	400	Radiative panel: NET HEAT FLUX = 112 kW/m²	NO	45.8	0.46	

Table 3.2: Water spray simulations

nr.	Mesh size (mm)	N_p (particles/s)	Mono- or Poly-disperse	Size distribution		Velocity distribution	Analysis
				Diameter (µm)	Gamma D	Particle velocity (m/s)	
22	50	5000	Poly-disperse	188	3.3	22	Size distribution analysis
23	50	5000	Poly-disperse	200	2.5	22	
24	50	5000	Poly-disperse	188	5	22	
25	50	5000	Poly-disperse	200	5	22	
26	50	5000	Poly-disperse	200	3.3	22	
27	50	5000	Poly-disperse	150	3.3	22	
28	50	5000	Poly-disperse	250	2.5	22	
29	50	5000	Poly-disperse	188	2.5	22	
30	50	5000	Poly-disperse	188	3.3	70	Velocity distribution analysis
31	50	5000	Poly-disperse	188	3.3	10	
32	50	5000	Poly-disperse	188	3.3	30	
33	50	5000	Poly-disperse	188	3.3	60	
34	50	5000	Poly-disperse	188	3.3	80	
35	50	5000	Poly-disperse	188	3.3	100	
36	10	5000	Poly-disperse	188	3.3	70	Sensitivity mesh analysis
37	20	5000	Poly-disperse	188	3.3	70	
38	40	5000	Poly-disperse	188	3.3	70	
39	80	5000	Poly-disperse	188	3.3	70	
40	40	10 000	Poly-disperse	188	3.3	70	Sensitivity analysis on the number of particles per second
41	40	50 000	Poly-disperse	188	3.3	70	
42	40	100 000	Poly-disperse	188	3.3	70	

Table 3.3: Combined simulations

nr.	Mesh size (mm)	N$_p$ (particles/s)	RA	Heating method	Water in steel present	k (W/(m.K))	c (kJ/(kg.K))	HTC (W/(m².K))	Mono- or Poly-disperse	Size distribution		Velocity distribution Particle velocity (m/s)	
										Diameter (µm)	Gamma D		
43	20	5000	200	RP:NHF=105 kW/m²	YES	45.8	0.46	300	Poly-disperse	188	3.3	70	Different HTC values of Poly- and Mono-disperse (bad mesh)
44	20	5000	200	RP:NHF=105 kW/m²	YES	45.8	0.46	600	Poly-disperse	188	3.3	70	
45	20	5000	200	RP:NHF=105 kW/m²	YES	45.8	0.46	800	Poly-disperse	188	3.3	70	
46	20	5000	200	RP:NHF=105 kW/m²	YES	45.8	0.46	1200	Poly-disperse	188	3.3	70	
47	20	5000	200	RP:NHF=105 kW/m²	YES	45.8	0.46	2000	Poly-disperse	188	3.3	70	
48	20	5000	200	RP:NHF=105 kW/m²	YES	45.8	0.46	60 000	Poly-disperse	188	3.3	70	
49	20	5000	200	RP:NHF=105 kW/m²	YES	45.8	0.46	-1	Poly-disperse	188	3.3	70	
50	20	5000	200	RP:NHF=105 kW/m²	YES	45.8	0.46	2000	Mono-disperse	188	/	70	
51	20	5000	200	RP:NHF=105 kW/m²	YES	45.8	0.46	300	Poly-disperse	188	3.3	70	Different HTC values of Poly- and Mono-disperse (good mesh)
52	20	5000	200	RP:NHF=105 kW/m²	YES	45.8	0.46	20 000	Poly-disperse	188	3.3	70	
53	20	5000	200	RP:NHF=105 kW/m²	YES	45.8	0.46	-1	Poly-disperse	188	3.3	70	
54	20	5000	200	RP:NHF=105 kW/m²	YES	45.8	0.46	20 000	Mono-disperse	188	/	70	
55	20	5000	200	RP:NHF=105 kW/m²	YES	45.8	0.46	-1	Mono-disperse	188	/	70	
56	20	5000	200	RP:NHF=105 kW/m²	YES	45.8	0.7	50 000	Poly-disperse	188	3.3	70	Final/Best

Chapter 4

Results

4.1 Hot Metallic plate

This section will go over the results of the hot metallic plate simulations.

4.1.1 Temperature difference cool and hot side steel plate

Firstly the simulation was done with a constant conductivity and specific heat for the steel. When analysing the results of the simulation with constant conductivity and specific heat for steel, the difference in temperature between the heated and cooler side of the steel plate was much smaller than in the experiment itself. This can be caused by multiple factors. For example the exact type of steel used in the experiment was unknown when producing this paper so an overall mild steel material was assumed, giving perhaps a higher conduction value than in reality. An emissivity of 1 is assumed because the steel plate is covered with black paint. Multiple simulations were done later with different conductivity values. But a reasonable value, to achieve the exact same temperature difference of 25 °C like in the experiment, was not reached so all simulations resulted in less temperature difference between the two sides of the steel plate than in reality.

4.1.2 Heating up to the required temperature

The multiple options of heating the steel plate were simulated and reviewed here 4.1, the main goal was to try and see if all simulations were able to heat up the steel plate to 600 °C and how agreeable they are with the experimental data.

The result in the graph above shows that all different heating options were able to heat the plate to a steady temperature of 600 °C in a fast enough time period, meaning with this that it was not slower than the experimental heating. This was the main objective. When looking more at the temperature rise for each option, the following analysis can be made. As expected the TMP_FRONT option for both the steel plate and radiative panel method gave an increase of around 590 °C over 3 seconds. The
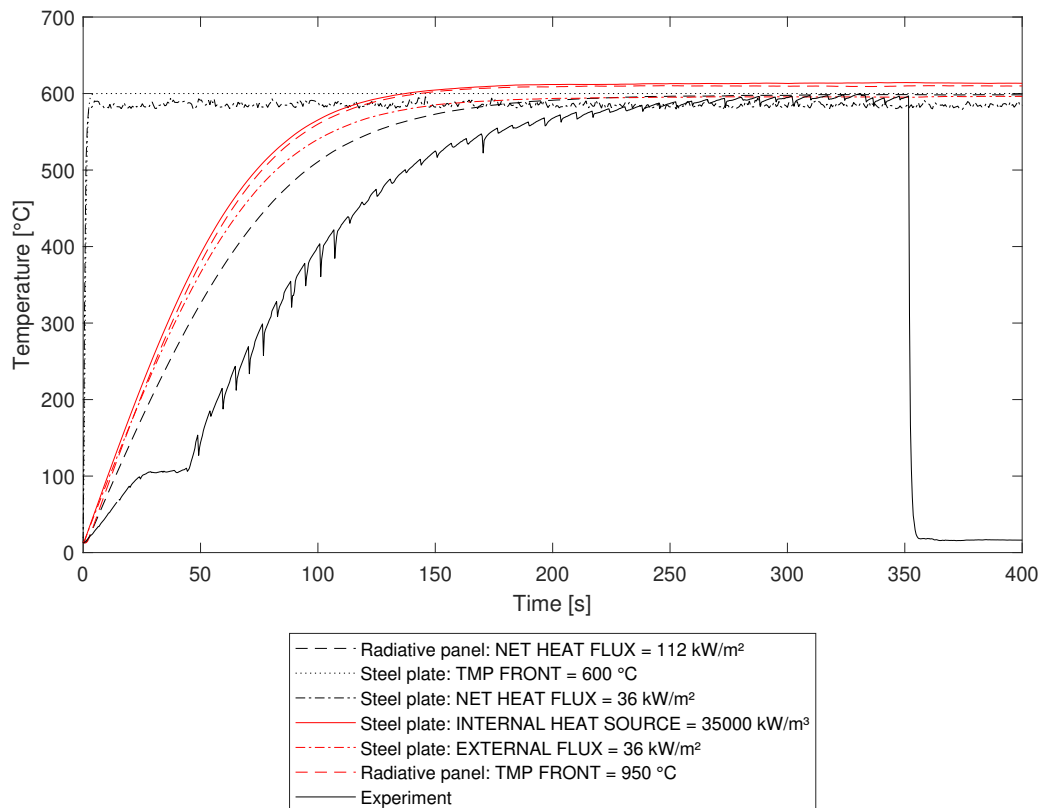
19

Figure 4.1: Wall temperature of cooled side steel plate with different heating methods in FDS

other options were able to follow the overall behaviour of the experimental temperature curve more correctly. Option 2b was the best representation of this curve. So the option of defining a value of 112 kW/m² for the net heat flux at the radiative panel, 2b, was chosen in the end for the rest of the simulations.

4.1.2.1 Water added to the steel plate

A clear observation is that the temperature is steady for a while during heating up. This occurs at 100 °C for approximately 15 seconds. The cause could be the evaporation of water inside the steel plate. This is further investigated and the simulation, of the radiative panel net heat flux only, is rerun with a second material present inside the steel plate, namely water. The effects of it are shown in the graph below 4.2. The net heat flux of the radiative panel is reduced from 112 to 105 kW/m² to keep a steady max wall temperature of 600 °C on the cool side.

After adding the water to the simulation, a clear plateau was achieved at around 100 °C, like in the experiment. The heating up after the plateau was faster than the simulation without water,
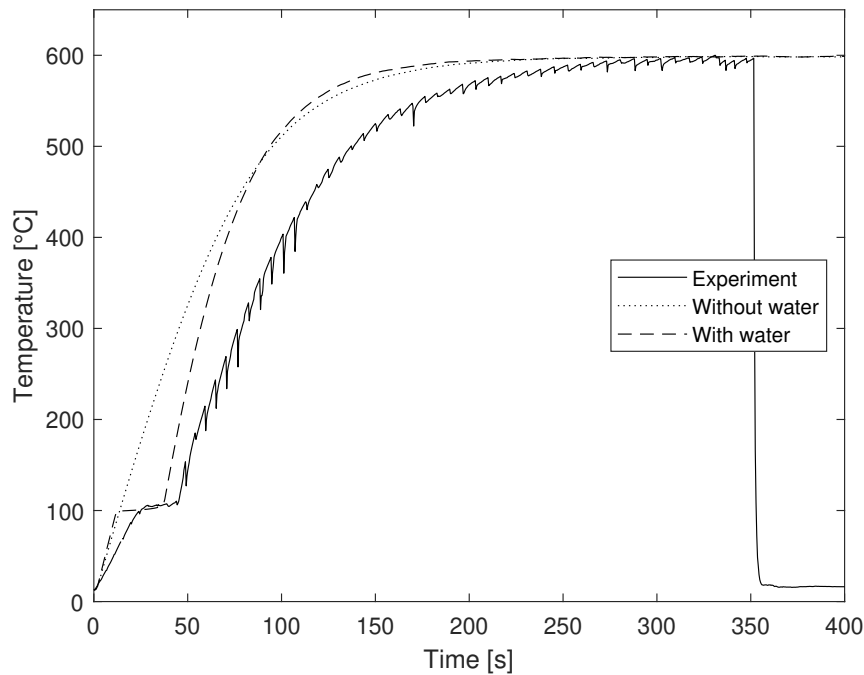
Figure 4.2: Difference in wall temperature of cooled side steel plate with and without the presence of water inside the solid

resulting in reaching a steady 600 °C around the same time for both simulations.

4.1.2.2   Variation of conductivity and specific heat of the steel

Another aspect that was further investigated and redefined is the conductivity and specific heat of the steel plate. In previous simulations this was assumed constant. But in reality the thermal conductivity, [19] [20], and specific heat, [21] [22], change as a function of temperature. As mentioned before, the exact type of steel used in the experiment is unknown and thus an assumption is made. The following graphs, 4.3a and 4.3b, show the used specific heat and thermal conductivity evolutions of steel.
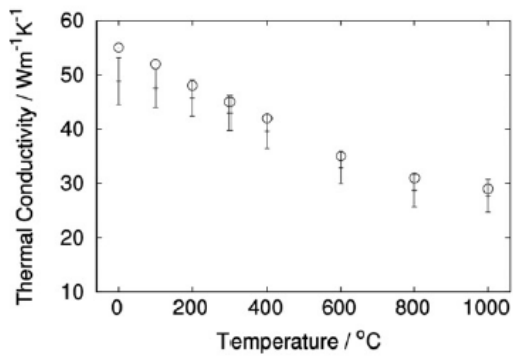
(a) Thermal conductivity from [20]
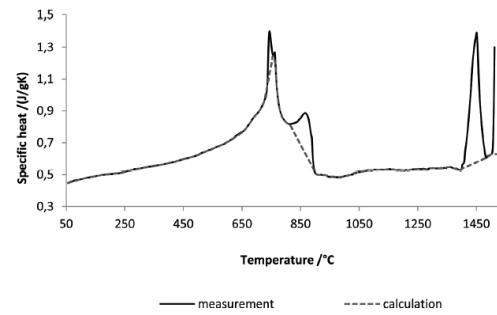
(b) Specific heat from [22]

Figure 4.3: Thermal conductivity and specific heat evolutions over temperature

The difference between the constant conductivity/specific heat of the steel plate and the variation of these values with temperature are shown in graph 4.4.

Figure 4.4: Difference in wall temperature of cooled side steel plate with and without a variation in conductivity and specific heat

To get extra information and an idea of what this conductivity and specific heat does to the heating up phase, multiple extra simulations were done where we increased and decreased the constant value of the conductivity and specific heat of steel, 4.5. This way it is also possible to get an idea of
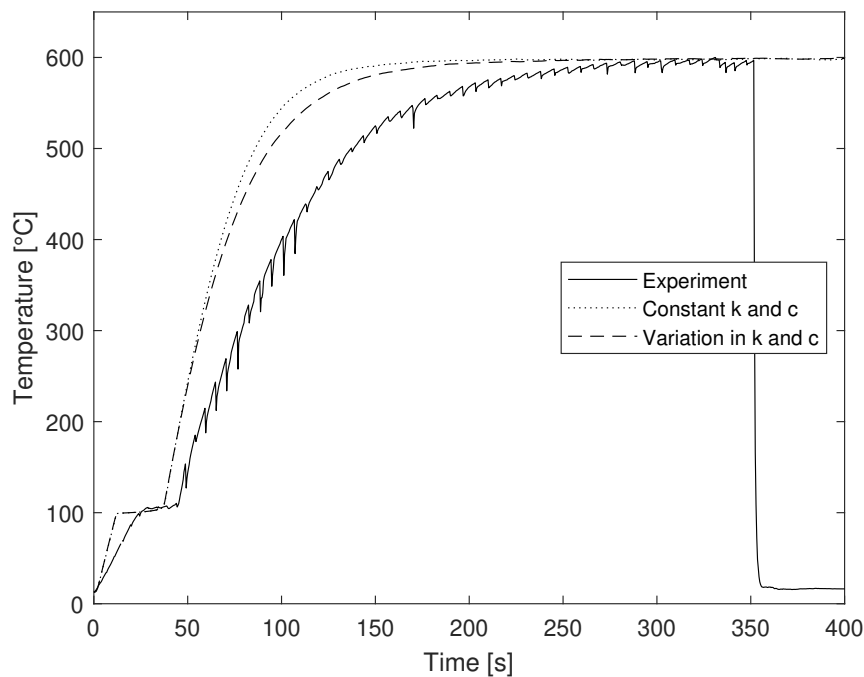
22

what the conductivity and specific heat needs to be in FDS to get an as close as possible result to the experimental data. This means that the values used here are not values supported by any paper or experiment but are values chosen by the author of this thesis.
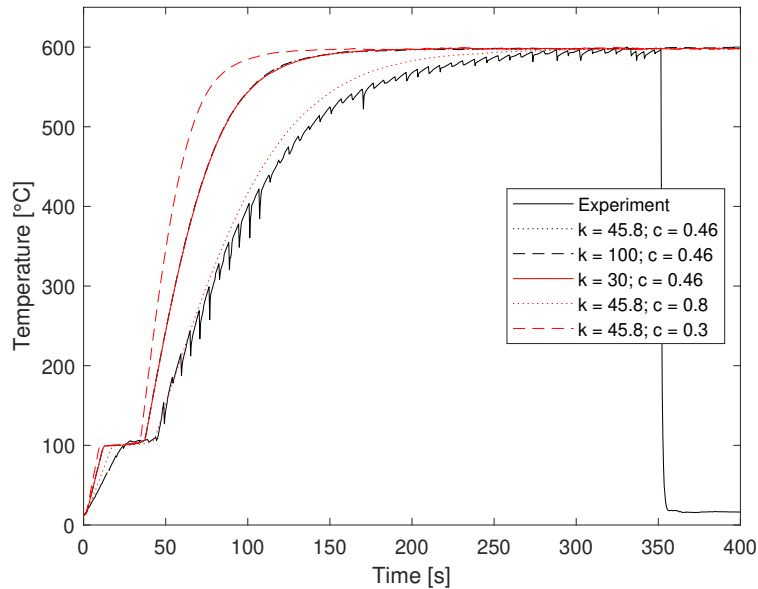

Figure 4.5: Different conductivity and specific heat simulations [k in W/(m.K) and c in kJ/(kg.K)]

A higher specific heat will result in a slower heating up and thus a better agreement with the experimental curve. Changing the conductivity does not differ for the heating up of the steel plate. This is due to the high conductivity values used here which results in making the steel plate thermally thin. Meaning that the heating up of the steel plate is mainly governed by the incident radiation and cooling due to re-radiation and convection. Increasing and decreasing the thermal conductivity does not change the outcome when using overall high values for k. The specific heat or c is much more important and influential in the calculations. The internal energy gained by the solid, considered here in the calculation for the heating of the plate, is calculated using the formula 4.1 found in [23].

$$\Delta E = m_{steel} c T_{steel} \tag{4.1}$$

where m_{steel} is the mass of the steel solid, c is the specific heat of the steel and T_{steel} is the steel temperature. Only one temperature is mentioned because the steel plate is thermally thin and thus it has no heat gradient throughout its thickness. The variation of this internal energy as a function of time is equal to the incident radiation minus the cooling due to re-radiation and convection. And this is the reason why the specific heat plays a crucial part in the temperature calculations of the steel plate.

All the data above has resulted in choosing a constant conductivity of 45.8 W/(m.K), as prescribed in [16], and a constant specific heat of 0.7 J/(g.K) which lies within the range provided in the literature 4.3b giving decent results similar to the experimental heating up data.

4.1.3 Sensitivity mesh size analysis

Here we go over the results of the sensitivity mesh size analysis.

After analysing and comparing the graphs of the temperature profiles, 4.6, we can conclude that the results of all the simulations follow globally the behaviour of the experiment (heating up phase only). The deviations mentioned in this sensitivity analyse part are average deviations with respect to the experimental data, between 300 and 350 seconds.

For the temperature results, see 4.6, the surprising conclusion is that the 40 mm mesh size has one of the lowest deviations together with the 10 mm cell size with an average deviation for the cool side of 0.47 % and 0.73 %. The deviation for the 20 mm mesh size is slightly larger with 2.05 % deviation from the experimental data. And last of all the 50 mm mesh size has the largest deviation of 3.59 %, as expected.
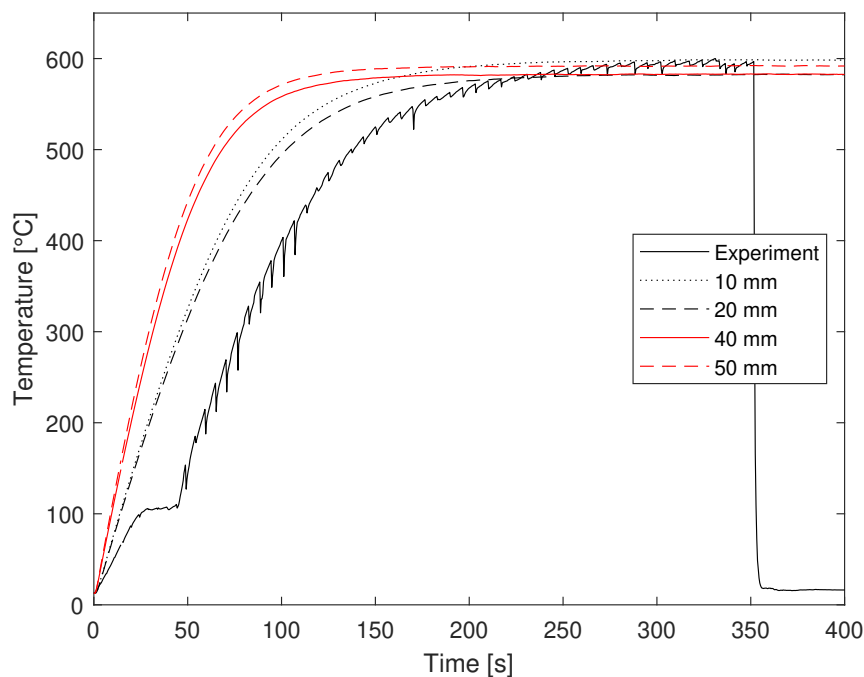
Figure 4.6: Wall temperature analysis steel plate with different mesh sizes, cool side

In the end a mesh size of 20 mm mesh was preferred. The deviations here were never significantly bigger than the 10 mm mesh size and the computational time can be accepted for the given results.

The 40 mm mesh size was not considered because the deviations of this simulation were unexpected and cannot directly be explained. This simulation could have some issues at the setup of the FDS file, with for example the geometry and mesh interaction and thus giving not so trustworthy results. But further investigation into the simulation itself was not done in this paper.

4.1.4 Sensitivity analysis on the number of radiation angles

In this section the radiation angles will be analysed on results sensitivity.

(a) RA 50 (b) RA 100 (c) RA 200 (d) RA 400
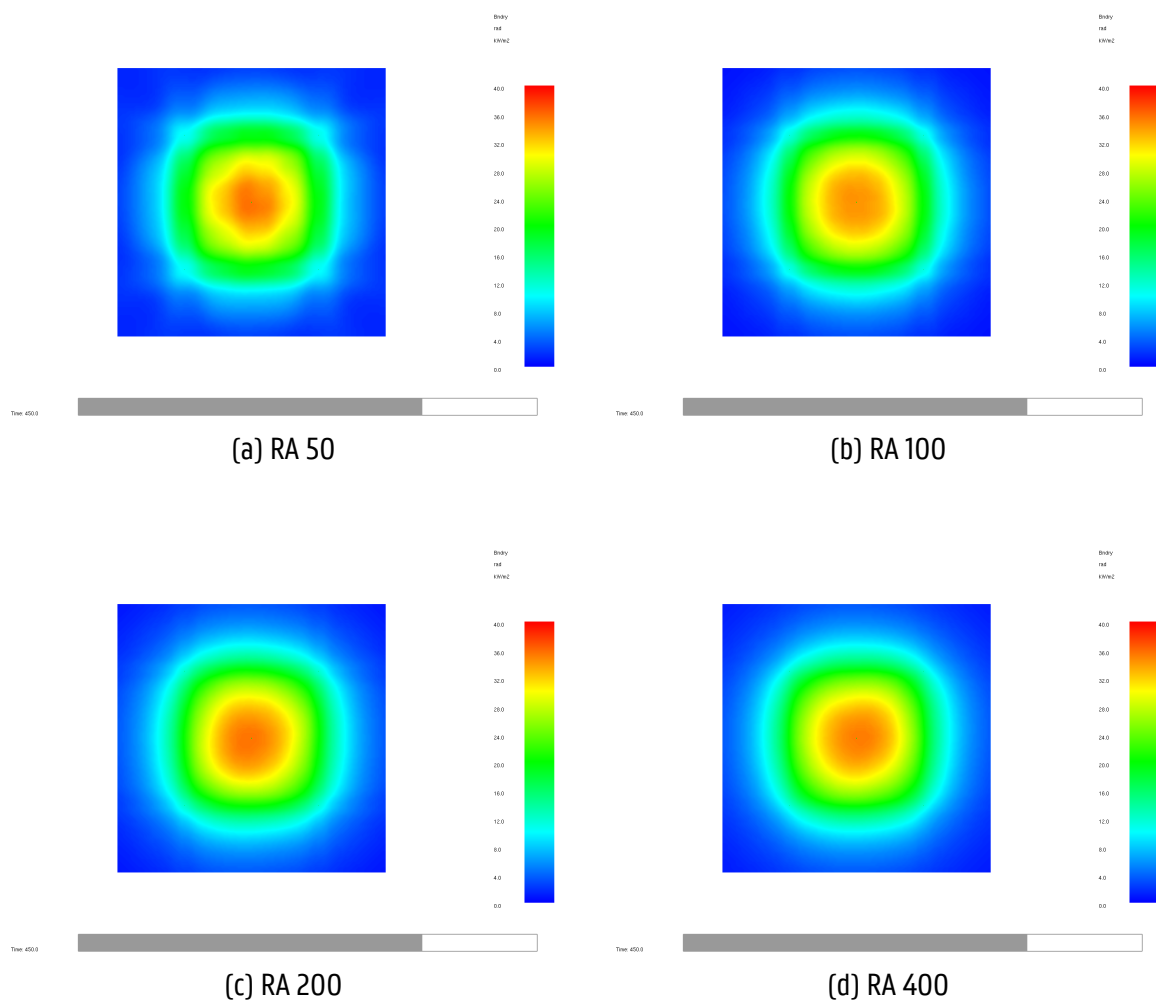
Figure 4.7: Radiative heat flux, bottom view, Heated side, time average (350-450 seconds) with different number of radiation angles with 10 mm mesh size

Looking at the different boundary files from SmokeView below, see 4.7, the overall boundary files look the same for every number of radiation angles. But the RA 50 does seem to have a less smooth circular pattern than the rest, especially at the corners. RA 100 is better in this aspect but not as

smooth as RA 200. So 200 radiation angels are chosen because of its very smooth pattern and almost no visual difference with RA 400 simulation.

An interesting observation that also occurred during the analysis of the different RA simulations was that for 50 radiation angles, the CPU time was longer than for example the higher 100 radiation angles simulation. This could be because more time is required to reach convergence in the numerical method that FDS uses.

Extra results with the different radiation angles simulations are found in 5. The results in wall temperature of all 4 simulations and the experiment, would lead to small average deviations of about 0.03 % minimum to a maximum of 2.4 % (for t_{sim} = 300 s - 350 s).

4.2 Water spray

4.2.1 Size distribution

When comparing multiple different simulations with different DIAMETER and GAMMA_D, a conclusion was made that the original input data of 188 μm for the D_{v50} and 3.3 for γ, found via the Matlab method, was the most similar to the experimental data, see 4.8. The comparison between this simulation and all the other ones can be seen in 5.
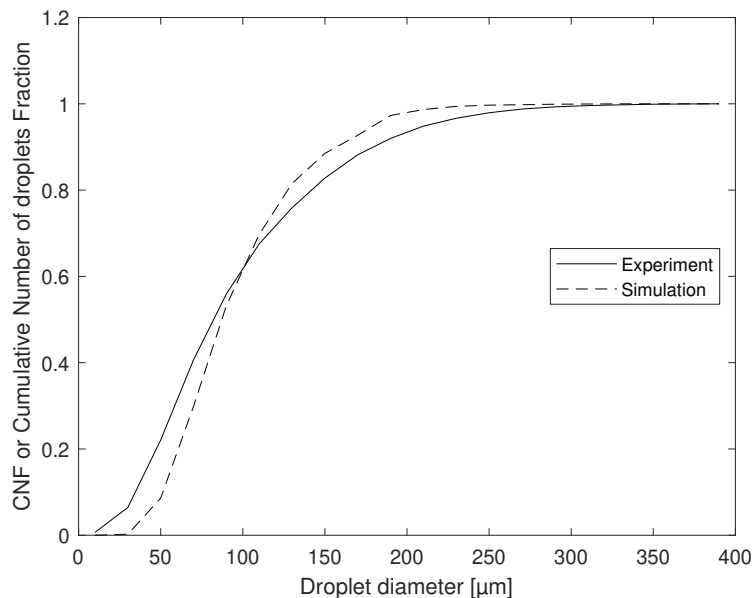

Figure 4.8: Size distributions measured at 50 cm below the nozzle for D_{v50} = 188 μm and γ = 3.3

The difference between poly and mono-disperse will be presented later in this paper.

4.2.2 Velocity distribution

After analysing multiple initial velocity histograms, see 5, an initial velocity of 70 m/s, see 4.9, is eventually chosen for all further simulation because this result corresponds best to the experimental curve.
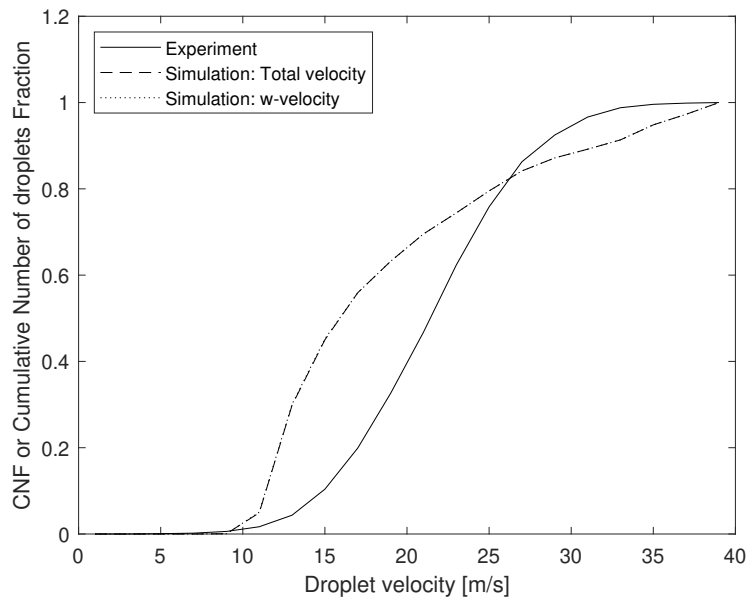
Figure 4.9: Velocity distributions measured at 50 cm below the nozzle for D_{v50} = 188 μm and γ = 3.3 and initial velocity of 70 m/s

The main focus of the graph above was the downwards w-velocity, as presumed, the experimental data also corresponds to the downwards velocity and not the overall velocity of the droplets. But this downwards w-velocity is in the center of the steel plate almost equal to the overall velocity. If these measurements are repeated more to the outside of the spray coverage area, the difference will be bigger due to the larger u- and v-droplet velocity components here. This will be addressed in more detail later in this paper.

4.2.3 Sensitivity mesh size analysis

Firstly we analyse the size distribution of the four different mesh size simulations, given in 4.10. This is overall the same for three simulations, the 20, 40 and 50 mm mesh size, thus resulting in the choice of picking the largest mesh of the three and computationally the less expensive simulation if needed. All three have an average deviation of 12 %. The 80 mm grid size has a larger deviation, 14 %, and has been discarded because of this.

Figure 4.10: Size distributions measured at 50 cm below the nozzle for different mesh sizes (D_{v50} = 188 μm; γ = 3.3; initial velocity of 70 m/s; N_p = 5000)

Secondly the analysis of the vertical velocity distribution with graph 4.11 is done. This results in a large difference between the 20 mm and the 40/50 mm mesh size simulation. To decide the best option out of the three a closer look at the average deviation was done, from 11 m/s until 39 m/s. The smallest deviation here is found for the 20 mm mesh size, giving this mesh size a little advantage over the other sizes. Again is the 80 mm mesh size not considered because of larger deviations and not following the same behaviour as the experiment.

Figure 4.11: Vertical velocity distributions measured at 50 cm below the nozzle for different mesh sizes (D_{v50} = 188 μm; γ = 3.3; initial velocity of 70 m/s; N_p = 5000)

For even further investigation on the mesh size, the vertical water mass flux was also measured for t_{sim} ranging from 460 seconds until 560 seconds. This gave the following result shown in 4.12. Showing no real converging or extreme deviations of any of the results we could not conclude a decent mesh size this way.

Now after analysing the multiple measurements taken for all different mesh size simulations, the 20 mm mesh size, with the most expected results as well as the lowest deviations overall, is chosen for further simulations.

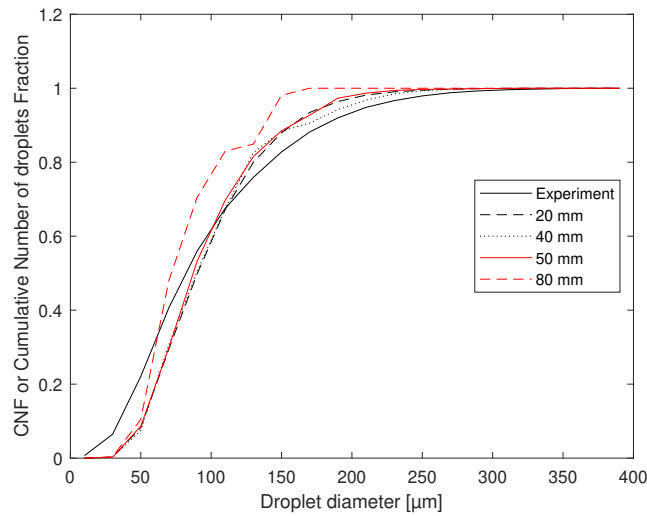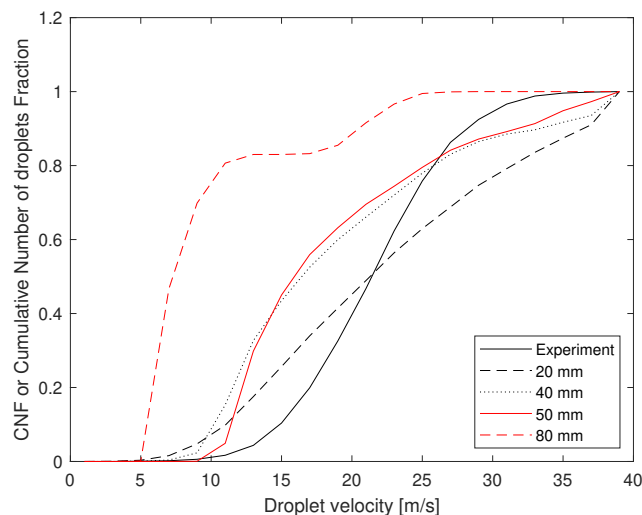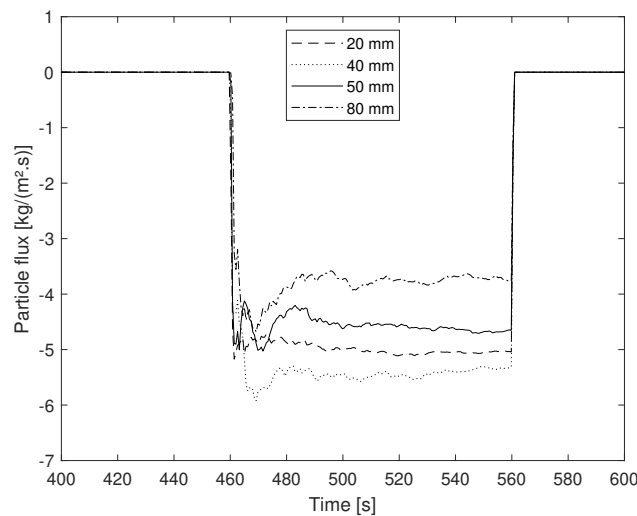Figure 4.12: Water mass flux in the vertical direction measured at 50 cm below the nozzle for different mesh sizes (D_{v50} = 188 µm; γ = 3.3; initial velocity of 70 m/s; N_p = 5000)

4.2.4   Sensitivity number of particles per second analysis

The results of this number of particles sensitivity analysis are shown below in 4.13.

The deviation for the size distribution ranges from 12 % for the N_p = 5000 to a minimum of 9 % for the N_p = 100000. This difference is so small that the simulation does not require a large number of particles to achieve decent results. What can be seen for higher PARTICLES_PER_SECOND is that the curve starts to behave with a somewhat ripply effect. This is even more visual in the velocity distribution 4.14. This can be the consequence of not enough bins in the PDPA setup in FDS or too large time periods between measurements. But the overall conclusion remains that no large N_p values are needed so the default 5000 number of particles per second simulation is sufficient.
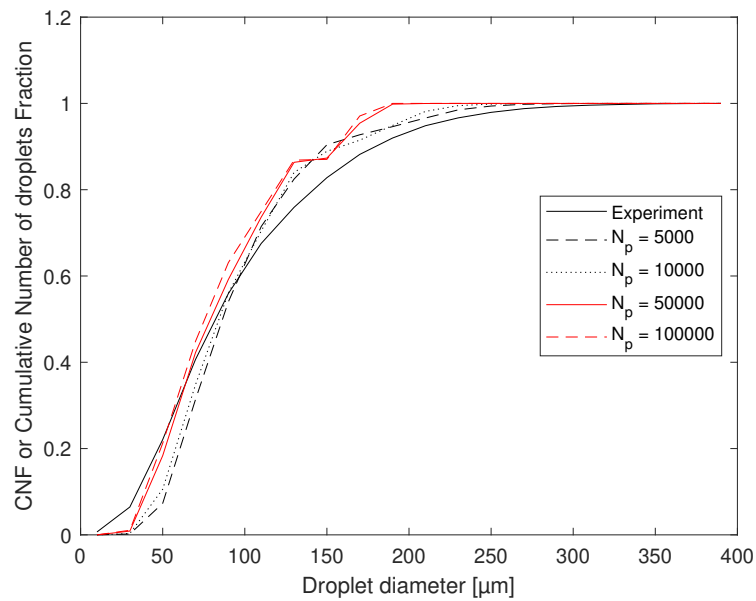
Figure 4.13: Size distributions measured at 50 cm below the nozzle for different N_p values (D_{v50} = 188 μm; γ = 3.3; initial velocity of 70 m/s)
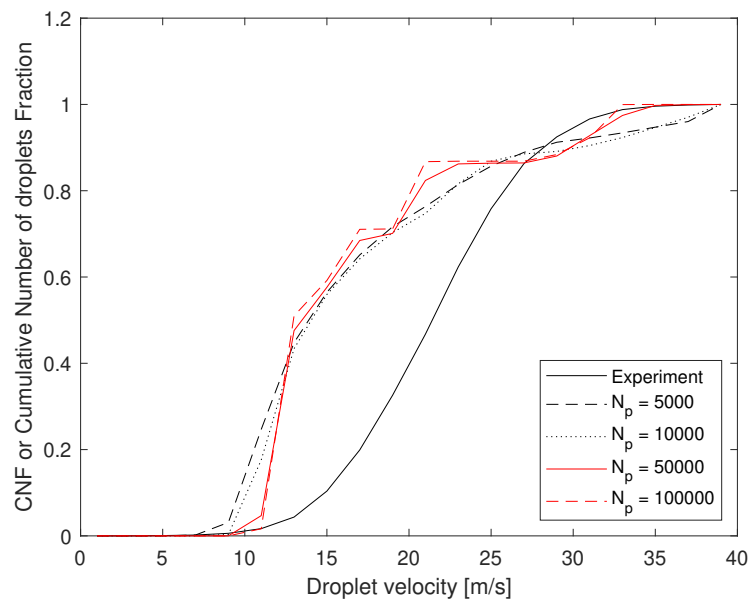
Figure 4.14: Vertical velocity distributions measured at 50 cm below the nozzle for different N_p values (D_{v50} = 188 μm; γ = 3.3; initial velocity of 70 m/s)

4.3   Interaction between the water spray and the hot metallic plate

In this section the results of the simulation combining the heated plate and water spray will be discussed.

4.3.1   Temperature

Firstly the temperature will be analysed during the simulation and compared to the experimental data. Especially the cool/top side wall temperature of the heated steel plate. This is one of the most important results, because this gives us the ability to analyse how well the surface wetting and thus cooling via water spray works in FDS compared to the experiment.

4.3.1.1   Temperature evolution during simulation

This first combined simulation was done without the presence of water inside the solid of the steel plate and with constant thermal conductivity as well as constant specific heat of the steel. This resulted in the following graph 4.15.
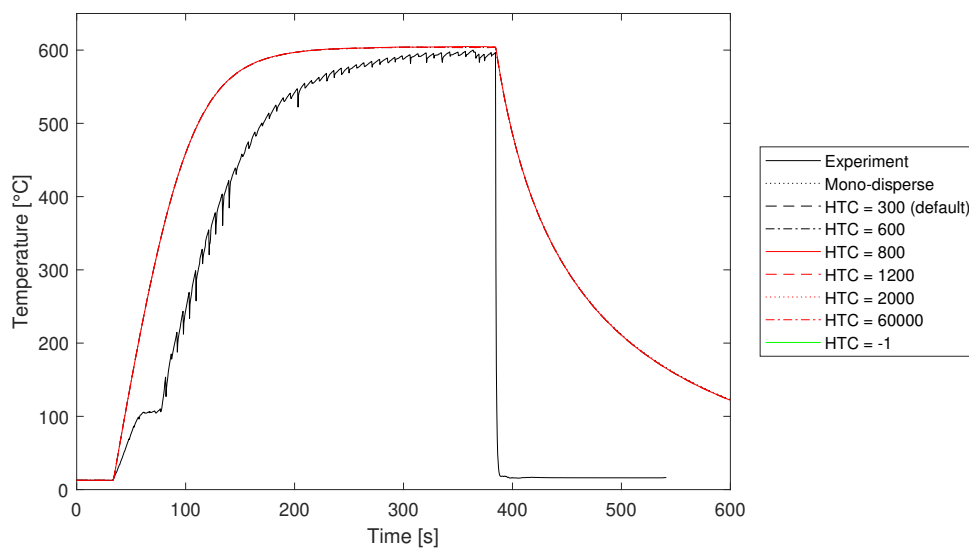
Figure 4.15: Temperature evolution cool side of the steel plate before adding water and RAMP (HTC in W/(m².K))

No plateau of the temperature was formed, as expected because no water was present inside the solid of the steel plate to take the energy for evaporation. But the most significant part of the graph above occurs after activation of the spray. The cooling was much slower in the simulated results

than in the experiment. This could be improved by increasing the heat transfer coefficient between the solid of the steel and the water droplets.

The experimental paper of Acem et al. [7] found very high heat flux and heat transfer coefficients when using the SU42 water spray nozzle, 4.17. Peaks of almost 70 000 W/(m².K) were reached and thus this explains why with our default heat transfer coefficient of 300 W/(m².K) we could never achieve the same cooling rate as in the experiment.

The cause of this malfunction in the simulation was the mesh size and the relations between the mesh and the objects in FDS. By using a mesh size where the objects created in FDS are in thickness smaller than the mesh size value, causes some sort of clipping and unexpected results. After altering the mesh size we get the results below 4.16
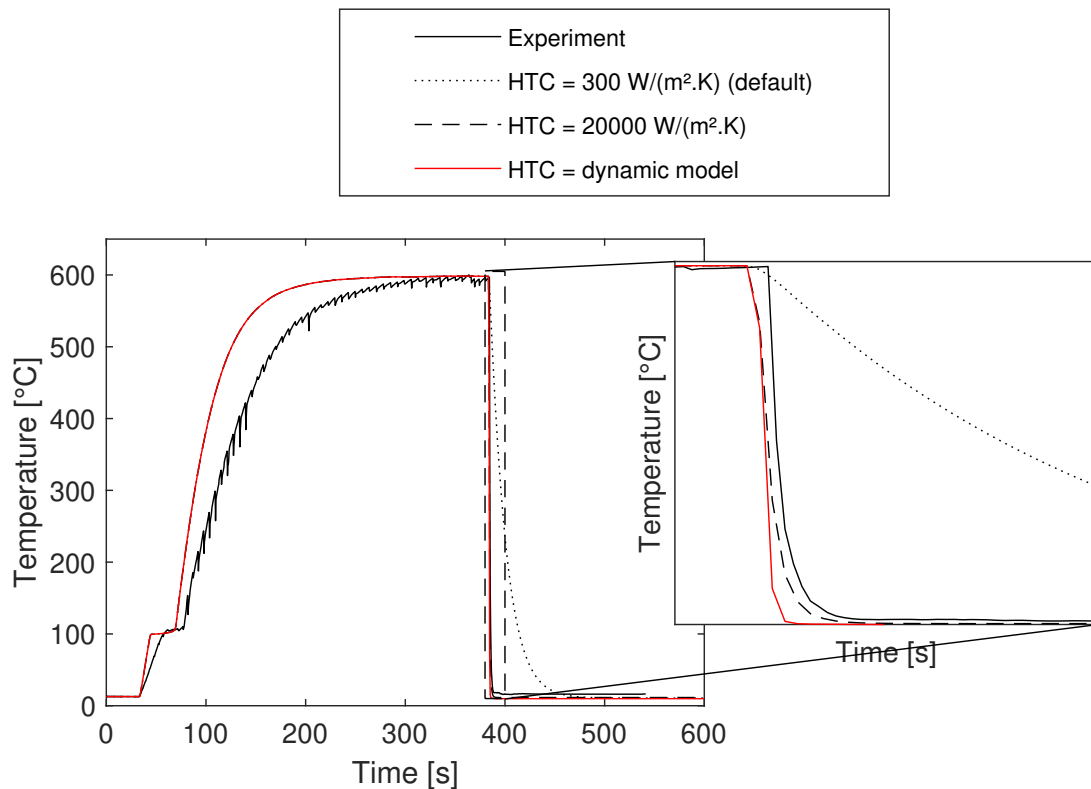
Figure 4.16: Temperature evolution measured at 50 cm below the nozzle for the cool side of the steel plate, water added and mesh fixed (HTC in W/(m².K))

Like mentioned before is HTC = -1 an experimental model which calculates the heat transfer coefficient dynamically. Meaning that the heat transfer coefficient will change with the temperature. More details about this model are not found in the FDS user guide, [15], or any other FDS guide. This

curve together with the heat transfer coefficient of 20 000 W/(m².K), corresponds the best with the experimental evolution of the temperature. Below, 4.1, are the times needed for the wall temperature of the cool side of the steel plate to reach ambient temperatures again Δt and the average cooling rates for each method. This table gives us a more detailed overview of the cooling. The difference between the experiment, 20 000 W/(m².K) HTC simulation and the experimental model simulation is now clearer. The high heat transfer coefficient of 20 000 W/(m².K) has a cooling rate 25 % smaller than the experiment. Increasing the HTC even higher to a value 25 000 would result in even more similar cooling rates. For the -1 simulation a much higher cooling rate than in the experiment can be seen, 70 % higher to be exact.

Table 4.1: Times for the cooled side to reach ambient temperature and cooling rates

	Simulation					Experiment
	Poly-disperse			Mono-disperse		
HTC (W/(m².K))	300	20 000	-1	20 000	-1	4.17
Δt (s)	88.8	5.40	2.40	6.00	2.40	4
Average cooling rate (°C/s)	6.59	108	245	97.6	245	144
CPU time (s)	196300	229300	249600	201900	210000	

The data reviewed above results in choosing for the 25000 heat transfer coefficient poly-disperse method. An important detail for the analysis above is that Δt and the average cooling rate have some inaccuracy due to the time step in which FDS outputs the device values. This time step, of 0.6 seconds, is relatively low in comparison to the total simulation time of 600 seconds. But when comparing this same time step value of 0.6 seconds to the cooling times of around 4 and 5 seconds we then see that this value is rather large. Thus the simulations result in not the most accurate cooling data. An option would be to increase the output data over a given time period via DT_DEVC. This is done for 1 simulation with a heat transfer coefficient of 50 000 W/(m².K) and with the use of a poly-disperse method. This resulted in a cooling rate of 108.23 °C/s, almost identical to the 20 000 W/(m².K) simulation above but now knowing that this result is much more accurate due to the smaller time step between measurements.
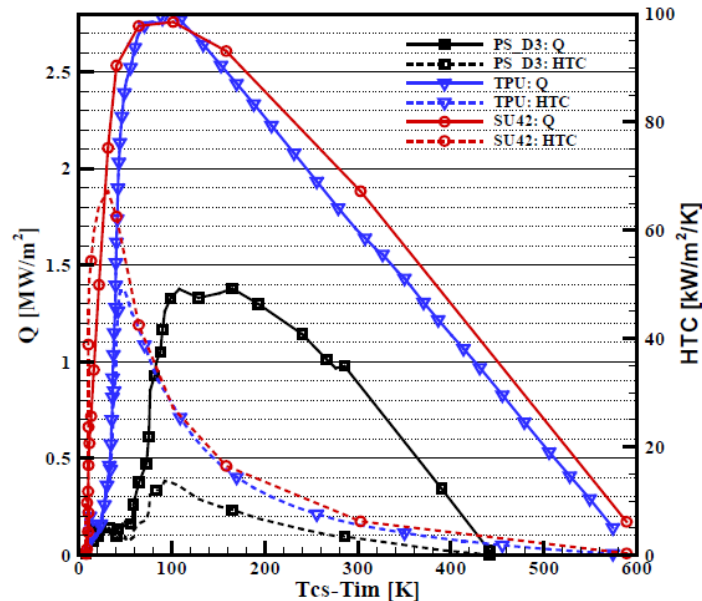
Figure 4.17: Heat fluxes (Q) and Heat transfer coefficients (HTC) experiment ([7])

4.3.1.2   Mono-disperse vs Poly-disperse

Like mentioned before there is also an option of choosing a single diameter for every droplet gen-erated in the simulation. The difference between the Poly- and Mono-disperse method is shown below for the experimental model (HTC = -1) and the simulation with a heat transfer coefficient of 20 000 W/(m².K), 4.18.

When looking at 4.1, the single droplet size simulation resulted in a cooling rate of 97.6 °C/s and the Poly-disperse method had a cooling rate of 108 °C/s. This difference is small, 10 % lower cooling rate for the Mono-disperse method. For a quick simulation and or simulating a given set-up without knowing anything about the droplet distribution, a mono-disperse method can be used to get overall decent results. When looking at the experimental method of -1 in FDS, no difference in cooling rates was observed.

The reason we would sometimes opt for the Mono-disperse method is that the CPU time is less than that of the Poly-disperse method. After doing these simulations the Mono-disperse method, for the 20 000 (W/(m².K)), was found to be 12 % or 7 hours and 36 minutes faster. Given that the entire simulation of the Poly-disperse method took around 2 days and 15 hours, the overall gain with the Mono-disperse method in CPU time is relatively low, but can still be preferred in some cases because of the overall decent results it delivers, especially when using the experimental model to calculate the heat transfer coefficient. Here the results of the Mono- and Poly-disperse method are the same and can be simulated 16 % or 11 hours faster with the single diameter droplet method.

34
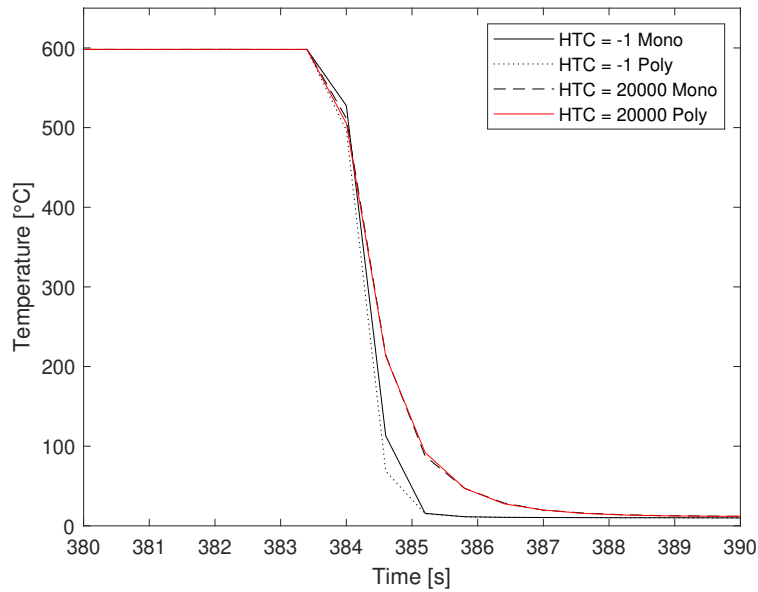
Figure 4.18: Temperature evolution of the cool side Mono- vs Poly-disperse (HTC in W/(m².K))

4.3.1.3   Slice files

Below we can see the average temperature slice files of the simulation between 200 s- 300 s, and between 390 s- 400 s, meaning before and after water spray activation 4.19. Resulting in expected Smokeview figures of the simulation.

(a) 200 s - 300 s
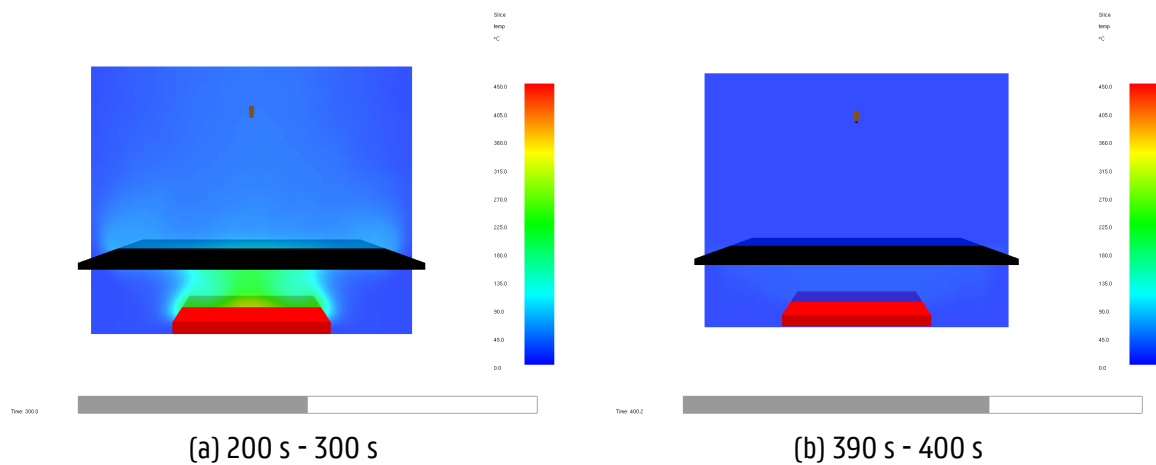
(b) 390 s - 400 s

Figure 4.19: Average temperature slice files
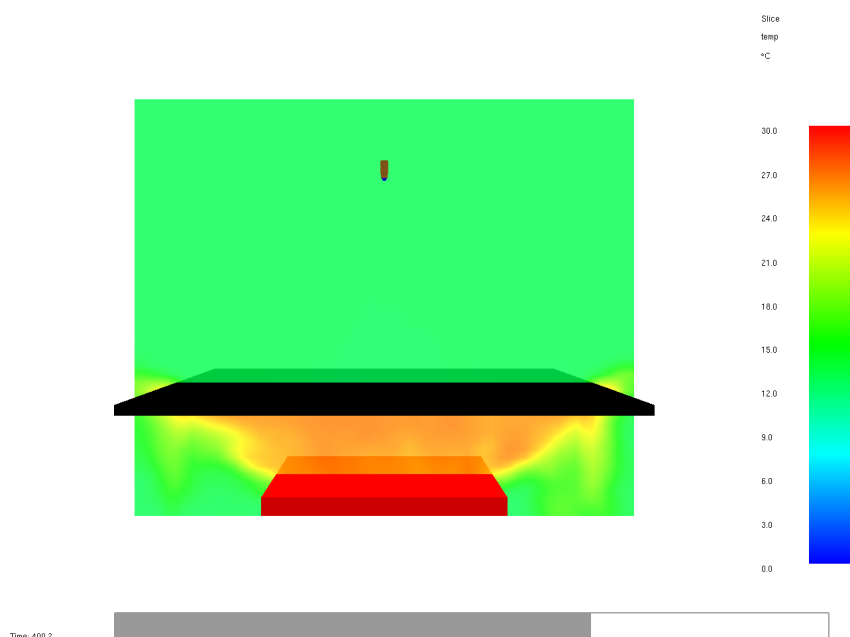
Figure 4.20: Average temperature slice file showing 0 to 40 °C from 390 s – 400 s

A closer look at lower temperatures of the slice file after activation of the water spray between 390 and 400 seconds shows that above the steel plate ambient temperatures are quickly reached, 4.20. Below the steel plate, some parts show slightly higher temperatures of around 25 – 30 °C, as expected, but even here the water spray system did a very effective job of cooling everything down in a very short period.

4.3.2   Velocity

In figure 4.21 is the velocity slice file of the 20 000 W/(m².K) heat transfer coefficient simulation shown at 400 s, so after water spray activation. Showing an air atomizing water spray with a small but effective spray coverage area. This spray coverage area will be discussed in more detail further in the paper.

The velocity measured at the cool side of the steel plate at different locations on the plate are shown in figure 4.22. Resulting in an expected lower vertical velocity than an overall velocity. The velocities of the water droplets decrease when moving further from the center of the steel plate until reaching a radial distance of around 0.09 m.   This is also observed by Thushadh in his paper [10] when going over the experimental data from Fu and his team [24].

This initial decrease in velocity is the consequence of increasing average droplets sizes when moving away from the center. The smaller droplets experience less aerodynamic drag due to their smaller cross section area and thus have less resistance when travelling through air. The reason why there are more smaller droplets in the middle of the spray than at the edges is mainly because these

small diameter droplets posses less momentum to counter the entrainment forces of the cooler air into the hot air plume.
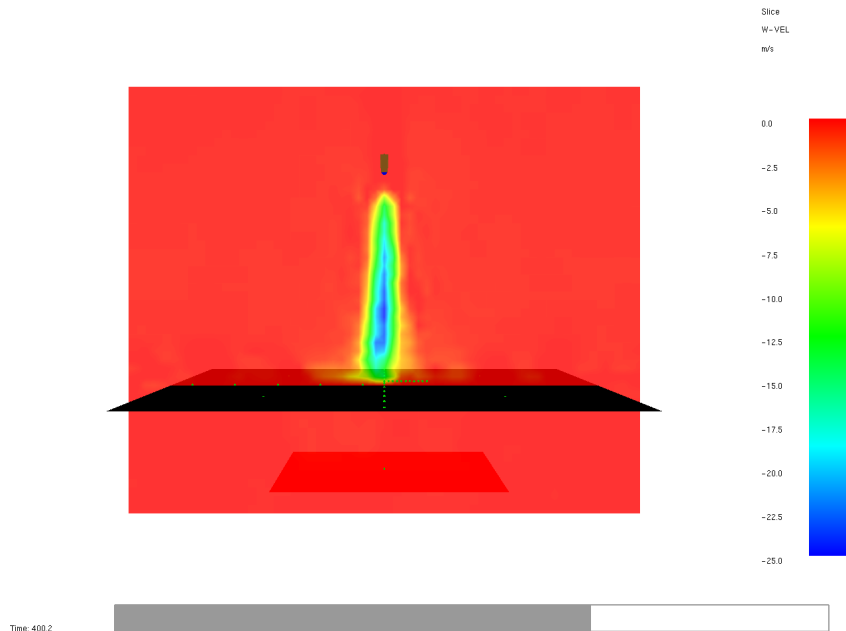
Figure 4.21: Velocity slice file at 400 s (HTC = 20 000 W/(m².K))
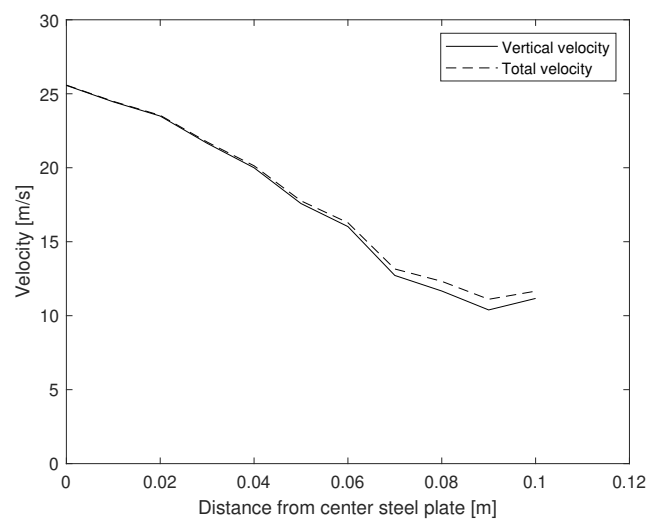
Figure 4.22: Average velocity at different distances from the center (HTC = 20 000 W/(m².K))

As mentioned before in this paper, the difference between the overall velocity and downwards velocity increases when measuring further from the center of the steel plate. This is an expected result due to the droplets, at a higher radial distance from the center, having larger u- and v-velocity components.

4.3.3   Heat fluxes

(a) Convective: 300 s

(b) Radiative: 300 s

(c) Convective: 385 s

(d) Radiative: 385 s

(e) Convective: 400 s

(f) Radiative: 400 s
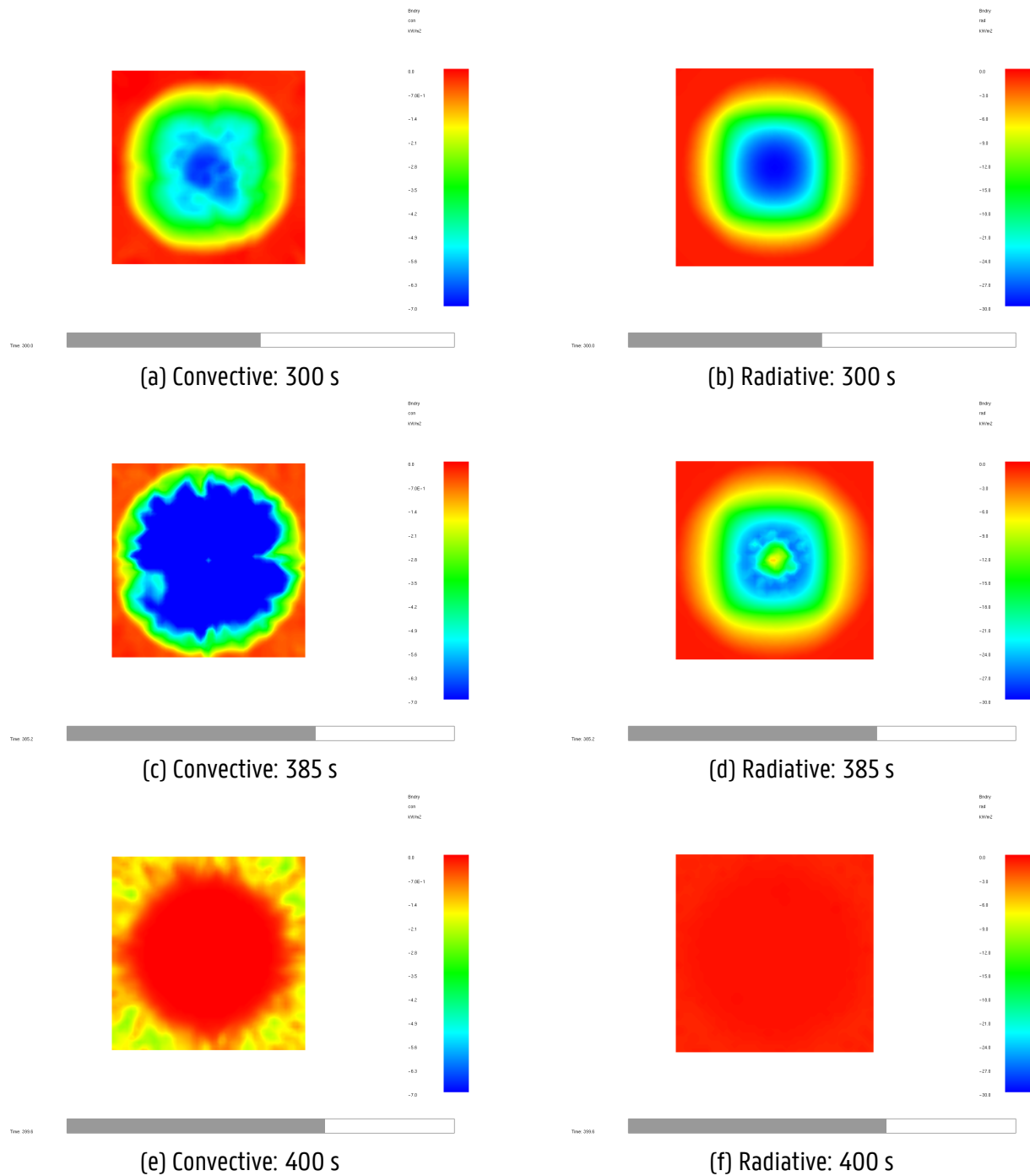
Figure 4.23: Heat fluxes seen from the top/cool side of the steel plate in Smokeview (HTC = 25 000 W/(m².K))

In figure 4.23 the Smokeview boundary heat flux file figures at 300 s, before activation of the spray, at 385 s, just after activation of the spray, and at 400 s, after activation of the spray are shown.

In the Smokeview figures above a high convective and radiative heat flux in the center of the plate can be seen, as expected, and this gradually decreases with higher radial distance from the center. At spray activation a larger area than before can be seen and with high convective heat fluxes. After this the convective heat flux at the center of the plate starts to decrease rapidly and this very fast decrease is observed starting at the center going outwards over the plate. The radiative heat flux does the exact same as the convective part does except the bigger area with high heat fluxes is not observed in this case. The radiative part drastically decreases in heat flux starting in the center and continues this trend going outwards.

Shown next is the heat fluxes evolution, at the center of the plate, during the simulation at the cool or top side of the steel plate, 4.24. Resulting in a clear drop in heat flux when the spray is activated.
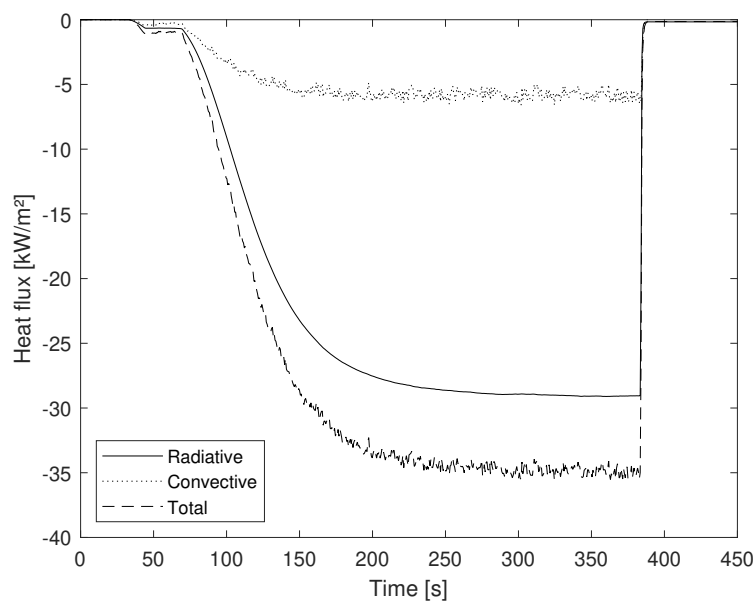
Figure 4.24: Heat fluxes at the cool side of the steel plate (HTC = 20 000 W/(m².K))

4.3.4   Coverage area

Next the coverage area of the water spray in the simulation is discussed and compared to the theoretical coverage area mentioned before in 2.2, being a circular area with a diameter of 18.5 cm. It is important to note that the theoretical coverage is calculated by using simple geometry equations. It predicts where the largest amount of the water spray droplets will land on a surface. There can be some droplets that will reach outside this theoretical coverage area, but this will not be effective for the overall surface cooling. It does not account for any fires or other influences present.

Meaning that accurately comparing this theoretical value with simulation coverage data is not possible where there is a fire or a heated surface at constant high temperatures during spray cooling. Because this thesis deals with a simulation with very fast cooling and where the PDPA values are measured long after the steel plate has cooled down, we can for the most part safely state that the results of our combined simulation can be compared with this theoretical value.

To get an idea of the simulated coverage area, multiple measurements can be done at different radial distances from the center of the steel plate to identify how far water droplets go and thus how big the coverage area is. This is possible with PDPA devices that measure for example the droplet size, downwards velocity or mass particle flux in the z direction.

For all three of the measured data, the average values found between 460 and 560 s of simulated time were used. The PDPA devices covered a distance from the center of the steel plate to 20 cm away from this center point. Keeping in mind that in the case of the simulations without hot metallic plate present, the devices were put at the exact location were the steel plate is located. This is, like mentioned before in the section about PDPA devices, not possible for the combined simulation. Here the devices were put 1 cm above the steel plate and thus are not located perfectly 50 cm below the spray, but in this case 49 cm.

4.3.4.1 Droplet diameter size over radial distance

This part goes over the droplets diameter sizes in μm.
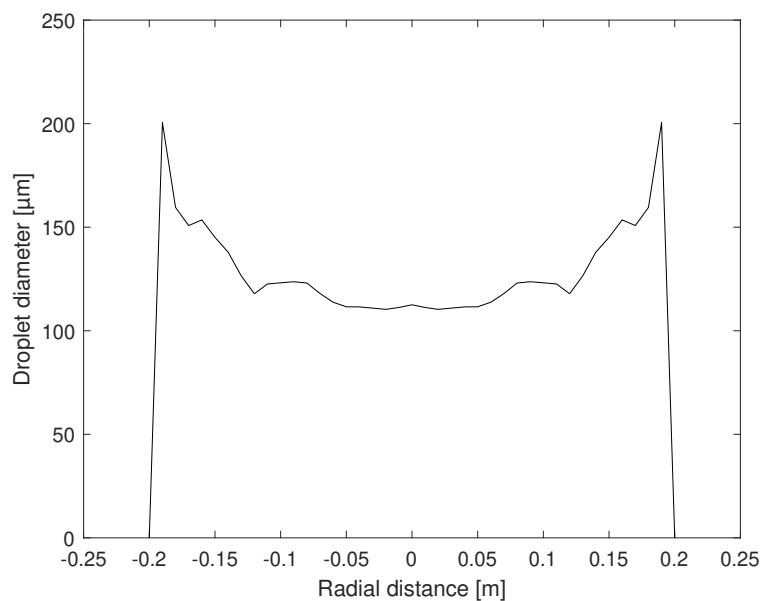
Figure 4.25: Average droplet diameter at different locations

From the results in figure 4.25 you can clearly see the the average droplet diameter rapidly drops to 0 after around 0.19 cm in either direction. Meaning that a circular coverage area with a diameter of 38 cm is assumed for this data. When comparing this to the theoretical coverage area diameter of 18.5 cm, the simulation yielded a more than two times larger coverage area. This may first seem as a surprise but can be explained. The reason for this is that this droplet diameter data only gives us the average particle size at a given distance from the center of the steel plate. It does not show any information on the amount of droplets at every location. Meaning that the measuring point far away from the center could only consist of a few bigger droplets and thus the spray cooling would have little effect here due to the low amount of water droplets. The particle mass flux in the z direction would be much better for analysing and estimating the coverage of the spray. This hypothesis is backed up with data of the number concentration of droplets measured at the same locations, see graph 4.26. Here we see that the PDPA measurements done at 0.13 meters and further have a very low volume sample compared to closer to the center measurements. The amount of droplets measured between a radial distance of 0.12 m and 0.2 m, are less than 1.3 % of all the droplets measured. Resulting in excluding these measurements when estimating the coverage area of the spray, and thus making it easier to presume that the estimated coverage area diameter, for this data, is 24 cm.
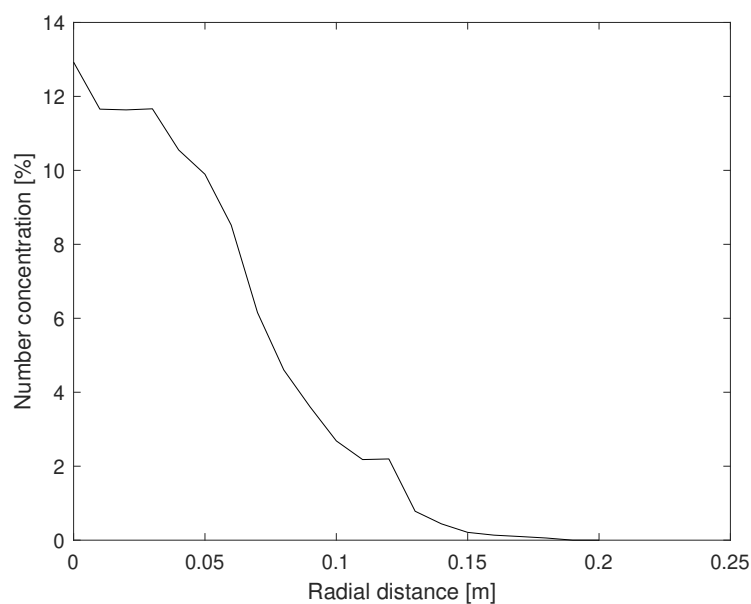
Figure 4.26: Number concentration of droplets at different locations

When looking at found data, the observation can be made that the size of the droplets increases when going further away from the middle of the spray. This has already been mentioned before in section 4.3.2 where the decrease of droplet velocities was linked to the increase of droplet diameter.

4.3.4.2 Downwards droplet velocity over radial distance

This part focuses on the downwards droplet velocities measured in m/s.
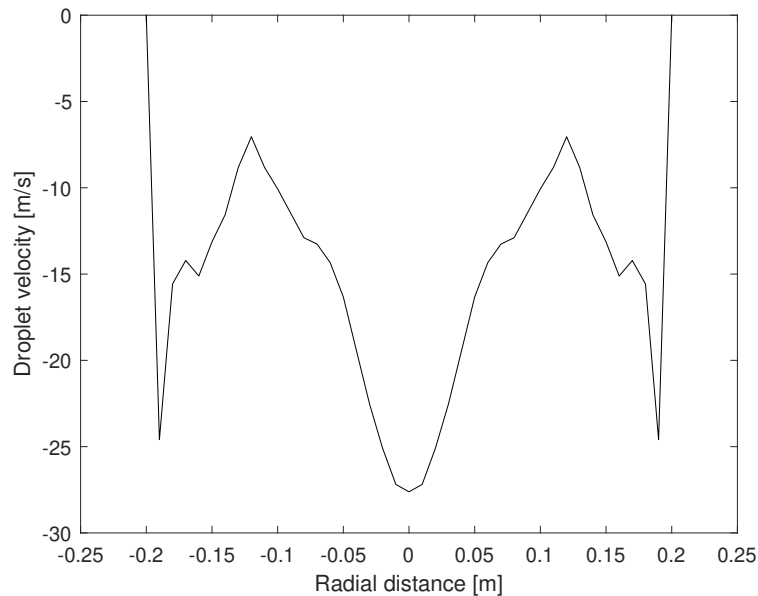
Figure 4.27: Average downwards droplet velocity at different locations

The figure 4.27 shows a fast drop in absolute vertical velocity values until reaching a distance of about 12 cm from the center axis of the spray, then it increases once more before finally going to 0. Again are the data of this section with the vertical velocity not very accurate or trustworthy to determine the actual coverage area. The same reasoning as for the droplet diameter can be used here. Thus the estimated coverage area diameter is again around 24 cm. Another interesting characteristic of this graph is the overall decrease of vertical velocity, when looking between -0.1 and 0.1 and when the vertical distance from the middle of the steel plate increases. Already indicated earlier in this paper, see 4.3.2.

4.3.4.3 Particle mass flux over radial distance

The last option for estimating the spray coverage area in the simulation is by going over the droplets mass flux in the downwards or z direction. This will probably result in the most accurate data for further estimating the coverage area of our spray.
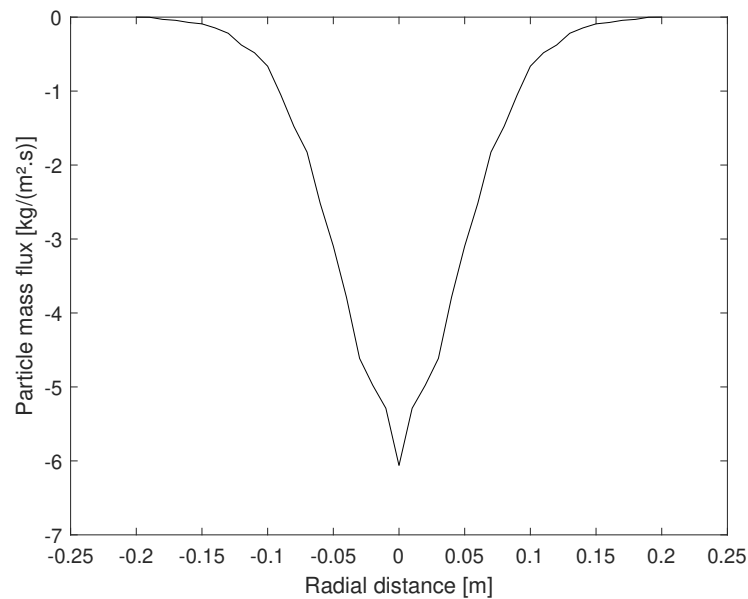
Figure 4.28: Average particle mass flux at different locations

From figure 4.28 we are able to predict a coverage area diameter of around 20 cm where water is detected, similar as seen in the droplet velocity and diameter graphs. For the water to be effective in cooling the material a sufficient amount of mass flux is needed. So assuming that a mass flux of under 1 kg/(m².s) is not effective enough to be seen as part of the coverage area of the spray. Thus an effective coverage area diameter would be 18 cm. The water "outside" of this circular diameter spray coverage is seen as droplets that are not contributing much to the surface cooling of objects.

This will probably be even more the case when measuring this data while there is a hot air or smoke plume present coming from a burning material or a heated surface. In this case, the entrainment of air into a plume could cause most of the "outside" droplets to be pushed to the center of the spray and/or the evaporation of "outside" droplets. Resulting in even less water mass flux at the outside of the spray. This assumption is in this paper not backed up by actual simulation output data due to limited time.

4.3.4.4   Conclusion for coverage area

So overall the conclusion is that the simulation has a good agreement with the real coverage area when keeping the assumption made before in mind. The presentation of the droplets diameter and vertical velocity data over radial distance was probably not very helpful for the coverage area prediction itself. Something that is interesting is when looking at the increase or decrease of measured values when moving to the edges of the water spray and what it means.

4.3.5 Boiling curve

In the introduction part of this thesis the boiling curve is mentioned and what this represents. The boiling curve, see 4.17, achieved in the experiments of Acem et al. [7] is also known. Thus replicating this boiling curve for the FDS simulations can be used to further compare it to the experimental one.

The boiling curve is defined by putting the heat flux in function of the excess surface temperature. This excess surface temperature is already explained in the introduction of this thesis and is the surface temperature of the cool side of the steel plate minus the saturated liquid temperature of the droplets. The surface temperature is known, 4.16, and the saturated temperature of the droplets can be estimated to be 100 °C, by creating a SmokeView figure and looking at the temperature of the water liquid just before evaporation, like done in 4.29.
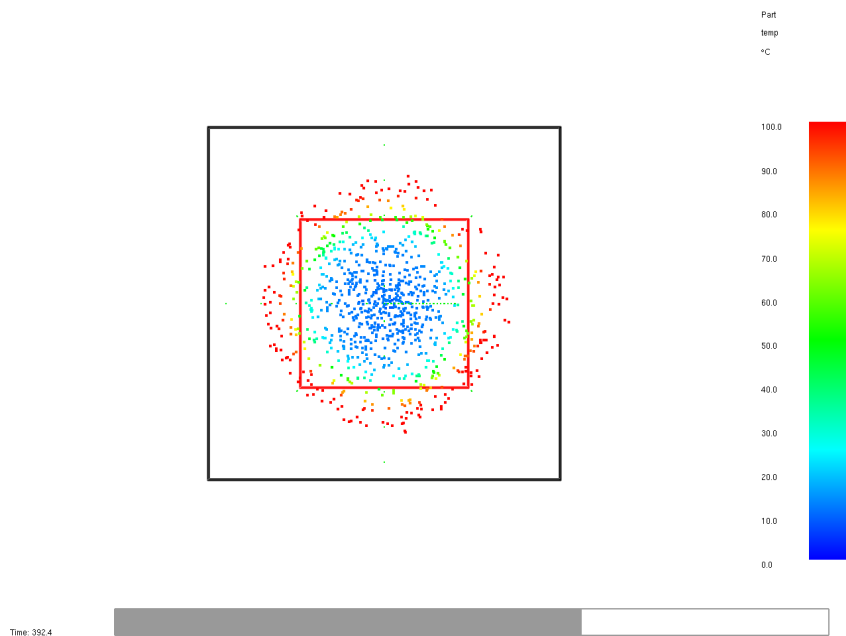
Figure 4.29: Particle temperature SmokeView file

The heat flux could be achieved by redoing the same calculations as done in the experiments. This is done by using the equation 4.2 to determine the heat flux.

$$\dot{q}'' = k\frac{\Delta T}{e} \tag{4.2}$$

where $\dot{q}''$ is the heat flux in (W/m²), k being the thermal conductivity of the steel in (W/(m.K)), ΔT is the temperature difference between the cool side and hot side of the steel plate in (K) and e is the thickness of the steel plate in (m).

Unfortunately in this simulation there are very small temperature differences between the cool and hot side of the steel plate due to an unknown thermal conductivity of steel value used in the

experiments, plus not being able to achieve the same temperature difference with FDS as found in the experiment with reasonable values for k. When calculating this in the same way for the simulation data, the following graph 4.30 is produced. Clearly showing lower heat flux values in the simulations due to the reasons mentioned above.
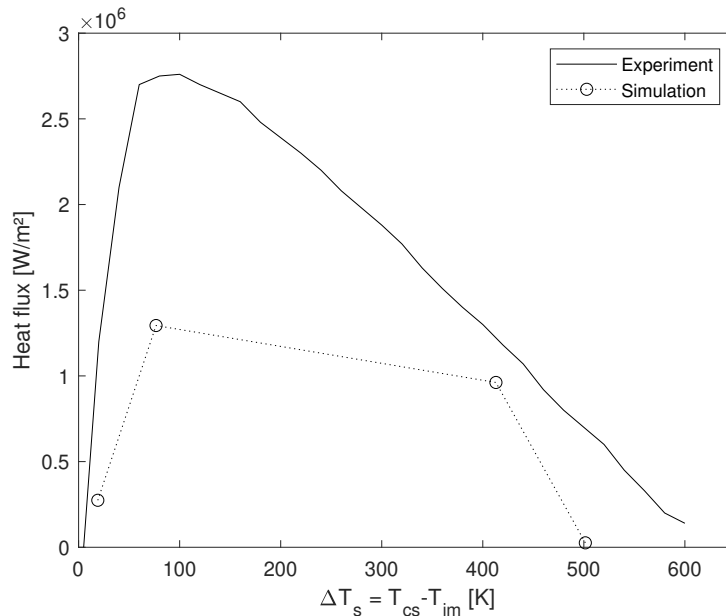
Figure 4.30: Boiling curve experiment vs simulation

4.3.6   Weber number

The focus in this section is put on the non-dimensional Weber number, explained in the introduction of this thesis. The values needed to calculate this Weber number are the density of water ρ being 1000 kg/m³ [15]. The surface tension of water σ being 0.0717 N/m at a temperature of 300 K and 0.0084 N/m at a temperature of 600 K [4]. The mean velocity of the droplets that can be calculated with the measured velocities of the simulation. And last of all the Sauter Mean Diameter or SMD that can be measured using PDPA devices. In 4.2 are the values found in Acem et al. paper and the simulated values.

Table 4.2: Sauter Mean Diameter, Mean velocity and Weber number

	SMD (µm)	Mean velocity (m/s)	Weber number
Experiment	171	22.4	1175
Simulation	147	20.0	824

Compared to the 1175 value for the Weber number Acem and his team found, [7], a lower value of 824 was measured here. The cause of this are the lower values found for SMD and mean velocity in the

simulations compared to the values of the experiment. In the set-up of the water spray system we were not able to exactly replicate the size and velocity distributions of the tests and were satisfied when acquiring a decent agreement to it. This caused the simulation to have an expected deviation in the end results, which is visible here.

Just as in the experiment our Weber number is significantly higher than the Weber value of 80 that is defined by Ito et al, [6], as the limit where droplets will rebound from the surface in the film boiling regime. Meaning that for Weber number values higher than 80 the rebound of the droplets is followed by disintegration into fine droplets, which is the case in this simulation too.

Chapter 5
Conclusion

When simulating only the hot metallic plate, the steel plate was able to reach a maximum temperature of around 598 °C for the cool or top side. This temperature was 596 °C in the experimental data, giving thus a very decent result. When looking at the heating up of the steel plate, again a good agreement with the experiment was achieved. 223.2 seconds were needed for the simulation to reach a, heated side steel plate, temperature of 590 °C. In the experiments was this achieved after 226 seconds, meaning only a difference of 2.8 seconds. For the temperature evolution at the cooled side of the steel plate were significantly bigger differences noticed. The simulation proved here to be much faster, 75 seconds to be exact, at attaining 590 °C in temperature. This is mostly due to insufficient information on the materials and their characteristic values used in the experiment and thus not having the same thermal conductivity and specific heat of steel.

After determining the droplet size and velocity distributions in the water spray simulation, a combined set-up in FDS produced cooling rates that were able to replicate the values received in the experiments. A cooling rate of 108 °C/s was achieved with the simulations meaning that ambient steel temperature at the cool side were measured only 5.3 seconds after activation of the spray. The experiment needed 4 seconds to achieve this, corresponding to a cooling rate of 144 °C/s.

The difference between simulating using a mono-disperse and a poly-disperse water spray was small, less than 10 % deviation, when using the high heat transfer coefficients and almost nihil when utilizing the experimental method of HTC = -1. Giving the conclusion that for some quick simulations, a mono-disperse method can be used to save CPU time. However overall, a poly-disperse water spray will output better results without significantly increasing the CPU time. With the used simulation set-up, 12 % better resembling results when using poly-disperse required 12 % more computational time.

For the Weber number, Sauter mean diameter and mean vertical velocity of the simulation, smaller values were found in comparison to the relating experimental values. This is presumed to be caused by the initial deviations of the droplet size and velocity distributions implemented in the set-up of the water spray in FDS. The coverage area that has been analysed via droplets size, vertical velocity

and mass flux, is found to be bigger than the presumed theoretical coverage area of the nozzle.

The validation study of the Fire Dynamics Simulator done in this paper proved that FDS is capable of providing accurate results for water cooling simulation on heated surfaces when using the proper input data. Thus only using the most basic set-up, without changing some default values, can result in significantly worse solutions. For example using the default value for the heat transfer coefficient between the solid and water droplets would result in a substantial decrease in cooling rate. Meaning that changing this 300 W/(m².K) value is crucial in acquiring acceptable results that are comparable to the experiments. This indicates that having the right input data, is very important when trying to recreate experiments with FDS, and not just trust the default settings. The mesh cell size and how the mesh is generated is a known important factor in making accurate CFD simulations, this was also experienced multiple times in the making of this paper.

Bibliography

[1] D. C. J V Murrell and P. Rock, "Experimental study of the thermal radiation attenuation of sprays from selected hydraulic nozzles," pp. 369–378, 1995.

[2] G. Grant, J. Brenton, and D. Drysdale, "Fire suppression by water sprays," *Progress in Energy and Combustion Science*, vol. 26, pp. 79–130, 2 Apr. 2000, ISSN: 0360-1285. DOI: 10.1016/S0360-1285(99)00012-X.

[3] J. Yin, S. Wang, X. Sang, *et al.*, "Spray cooling as a high-efficient thermal management solution: A review," *Energies*, vol. 15, no. 22, 2022, ISSN: 1996-1073. DOI: 10.3390/en15228547. [Online]. Available: https://www.mdpi.com/1996-1073/15/22/8547.

[4] "Heat transfer: A. bejan john wiley and sons, 675 pp. 75.95," *International Journal of Heat and Fluid Flow*, vol. 15, p. 341, 4 Aug. 1994, ISSN: 0142-727X. DOI: 10.1016/0142-727X(94)90021-3. [Online]. Available: https://linkinghub.elsevier.com/retrieve/pii/0142727X94900213.

[5] J. Rymkiewicz and Z. Zapalowicz, "Analysis of the evaporation process for water droplet on flat heated surface," *International Communications in Heat and Mass Transfer*, vol. 20, pp. 687–697, 5 Sep. 1993, ISSN: 0735-1933. DOI: 10.1016/0735-1933(93)90080-F.

[6] T. Ito, Y. Takata, M. Mousa, and H. Yoshikai, "Studies on the water cooling of hot surfaces experiment of spray cooling," English, *Memoirs of the Graduate School of Engineering, Kyushu University*, vol. 51, no. 2, pp. 119–144, Jun. 1991, ISSN: 1345-868X.

[7] A. Z., M. R., D. V., *et al.*, "Water sprays cooling of a hot metallic plate,"

[8] A. Labergue, M. Gradeck, and F. Lemoine, "Comparative study of the cooling of a hot temperature surface using sprays and liquid jets," *International Journal of Heat and Mass Transfer*, vol. 81, pp. 889–900, Feb. 2015, ISSN: 0017-9310. DOI: 10.1016/J.IJHEATMASSTRANSFER.2014.11.018.

[9] T. Incorporated, *Phase Doppler Particle Analyzer (PDPA)/ Laser Doppler Velocimeter (LDV): Operations Manual revision E*. 2006. [Online]. Available: https://www.eng.uwo.ca/research/afm/documents/tsi1.pdf.

[10]   T. Wijesekere, "Numerical modelling of water spray impingement cooling," 2021.

[11]   P. P. Rubini, *Powerpoint notes in simulation of fires in enclosures*, Feb. 2021.

[12]   M. Mitsutsuka and K. Fukuda, "Cooling characteristics and heat transfer coefficients during fog cooling of hot steel plates," vol. 21, pp. 689–698, 1981.

[13]   S. S. Co., *Automatic and air atomizing spray nozzles*. [Online]. Available: https://www.spray.com/-/media/dam/industrial/usa/sales-material/catalog/cat76a-aa_metric.pdf (visited on 01/18/2023).

[14]   A. Systems, *Sprayspy labline*. [Online]. Available: https://www.aom-systems.com/en/?page_id=2116 (visited on 02/11/2023).

[15]   K. McGrattan, S. Hostikka, J. Floyd, R. McDermott, and M. Vanella, "Fire dynamics simulator user's guide, nist special publication 1019," in 6th ed. NIST National Institute of Standards and Technology, 2021.

[16]   D. Drysdale, *An Introduction to Fire Dynamics*, 3rd ed. John Wiley and Sons Ltd, 2011.

[17]   R. C. Reid, J. M. Prausnitz, and B. E. Poling, *The Properties of Gases and Liquids*, 4th ed. McGraw-Hill, Inc., 1987.

[18]   T. Beji, S. E. Zadeh, G. Maragkos, and B. Merci, "Influence of the particle injection rate, droplet size distribution and volume flux angular distribution on the results and computational time of water spray cfd simulations,"

[19]   S. M. Shelton, "Thermal conductivity of some irons and steels over the temperature range 100 to 500 c, research paper rp669," *Bureau of Standards Journal of Research*, vol. 12, pp. 441–449, 1934.

[20]   M. J. Peet, H. S. Hasan, and H. K. Bhadeshia, "Prediction of thermal conductivity of steel," *International Journal of Heat and Mass Transfer*, vol. 54, pp. 2602–2608, 11-12 May 2011, ISSN: 0017-9310. DOI: 10.1016/J.IJHEATMASSTRANSFER.2011.01.025.

[21]   S. Umino, "On the specific heat of carbon steels," pp. 331–369, [Online]. Available: https://core.ac.uk/download/14513985.pdf.

[22]   T. Kargul, E. Wielgosz, and J. Falkus, "Application of thermal analysis tests results in the numerical simulations of continuous casting process," *Archives of Metallurgy and Materials*, vol. 60, p. 221, Mar. 2015. DOI: 10.1515/amm-2015-0035.

[23]   K. McGrattan, S. Hostikka, J. Floyd, R. McDermott, and M. Vanella, "Fire dynamics simulator technical reference guide volume 2: Verification, nist special publication 1018-2," in 6th ed. NIST National Institute of Standards and Technology, 2021.

[24]   C. Fu, P. E. Sojka, and Y. R. Sivathanu, "On the interaction between evaporating sprays and heated surfaces," *Proceedings of the 12th Annual Conference on Liquid Atomization and Spray Systems, Indianapolis, IN*,

Appendices

Appendix A

FDS file: Combination of water spray system and heated plate

```
&HEAD CHID='THESIS_CEDRIC_FINAL_COMBINED_SIMULATION',
TITLE='THESIS_CEDRIC_FINAL_COMBINED_SIMULATION' /

&TIME T_END=600 /

&MESH ID='mesh1', IJK=60,60,10, XB=-0.6,0.6,-0.6,0.6,-0.31,-0.11, MPI_PROCESS=0 / 0.02 m
or 20 mm mesh size
&MESH ID='mesh2', IJK=60,60,10, XB=-0.6,0.6,-0.6,0.6,-0.11,0.09, MPI_PROCESS=1 /
&MESH ID='mesh3', IJK=60,60,10, XB=-0.6,0.6,-0.6,0.6,0.09,0.29, MPI_PROCESS=2 /
&MESH ID='mesh4', IJK=60,60,10, XB=-0.6,0.6,-0.6,0.6,0.29,0.49, MPI_PROCESS=3 /
&MESH ID='mesh5', IJK=60,60,10, XB=-0.6,0.6,-0.6,0.6,0.49,0.69, MPI_PROCESS=4 /

//////////////////////// Hot metallic plate part ////////////////////////

&RADI NUMBER_RADIATION_ANGLES = 200/

&MISC TMPA=12.75 /

&OBST XB= -0.5, 0.5, -0.5, 0.5, -0.01, 0.01, SURF_ID='Hot metallic plate', COLOR='BLACK'/

&OBST XB= -0.26, 0.26, -0.26, 0.26, -0.23, -0.21, SURF_ID='Radiative panel', COLOR='RED'/

&SPEC ID='METHANE' /

&MATL ID='Steel'
        SPECIFIC_HEAT         = 0.7
        CONDUCTIVITY          = 45.8
        DENSITY               = 7850 / cond in W/m.K ; spec heat in kJ/kg.K; density in
kg/m³;

&MATL ID = 'WATER'
        EMISSIVITY            = 1.0
        DENSITY               = 1000.
        CONDUCTIVITY          = 0.20
        SPECIFIC_HEAT         = 4.184
        N_REACTIONS           = 1
        REFERENCE_TEMPERATURE = 100.
        PYROLYSIS_RANGE       = 10.
```

```
        NU_SPEC                = 1.
        SPEC_ID                = 'METHANE'
        HEAT_OF_REACTION       = 2500.  /


&SURF ID = 'Hot metallic plate'
        MATL_ID(1,1:2)         = 'Steel','WATER'
        MATL_MASS_FRACTION(1,1:2) = 0.95,0.05
        THICKNESS              = 0.002/

&SURF ID = 'Radiative panel'
        NET_HEAT_FLUX          = 110
        RAMP_Q                 = 'NHFRAMP'
        BACKING                = 'INSULATED'/

&RAMP ID='NHFRAMP', T=0.0, F=0.0 /
&RAMP ID='NHFRAMP', T=32.7, F=0.0 /
&RAMP ID='NHFRAMP', T=32.8, F=1.0 /
&RAMP ID='NHFRAMP', T=384.3, F=1.0 /
&RAMP ID='NHFRAMP', T=384.4, F=0.0 / F is percentage and T is time


///////////////////// Water spray part /////////////////////

&SPEC ID = 'WATER VAPOR' /

&PART ID = 'Watermist', SPEC_ID='WATER VAPOR', QUANTITIES = 'PARTICLE DIAMETER', 'PARTICLE
TEMPERATURE', 'PARTICLE VELOCITY', DIAMETER = 188, GAMMA_D = 3.3, HEAT_TRANSFER_COEFFICIENT_SOLID
= 50000/

&PROP ID='sprinkler',
        PART_ID                = 'Watermist',
        OFFSET                 = 0.02,
        SPRAY_ANGLE            = 0,21,
        FLOW_RATE              = 4.6,
        PARTICLE_VELOCITY      = 70,
        FLOW_RAMP              = 'SPRAMP',
        PARTICLES_PER_SECOND = 5000.0 /

&RAMP ID='SPRAMP', T=0.0, F=0.0 /
&RAMP ID='SPRAMP', T=1.0, F=1.0 / F is percentage and T is time

&DEVC ID='SPR', XYZ=0.0,0.0,0.51, ORIENTATION=0,0,-1, PROP_ID='sprinkler', QUANTITY='TIME',
SETPOINT=383.4 /
```

```
&VENT DB='XMIN', SURF_ID='OPEN' /
&VENT DB='XMAX', SURF_ID='OPEN' /
&VENT DB='YMIN', SURF_ID='OPEN' /
&VENT DB='YMAX', SURF_ID='OPEN' /
&VENT DB='ZMIN', SURF_ID='OPEN' /
&VENT DB='ZMAX', SURF_ID='OPEN' /


///////////////////// Slice files /////////////////////////

&SLCF PBZ= -0.01, QUANTITY='TEMPERATURE' /
&SLCF PBZ= 0.01, QUANTITY='TEMPERATURE' /
&SLCF PBY= 0, QUANTITY='TEMPERATURE' /
&SLCF PBY= 0, QUANTITY='W-VELOCITY' /


///////////////////// Devices wall temperature ///////////////////////

&DEVC ID='WTHOT', XYZ= 0, 0, -0.01, QUANTITY='WALL TEMPERATURE', IOR = -3 / me grid veranderen
&DEVC ID='WTCOOL', XYZ= 0, 0, 0.01, QUANTITY='WALL TEMPERATURE', IOR = 3 /


&DEVC ID='WT1', XYZ= -0.25, -0.25, -0.01, QUANTITY='WALL TEMPERATURE', IOR = -3  /
&DEVC ID='WT2', XYZ= -0.25, 0.25, -0.01, QUANTITY='WALL TEMPERATURE', IOR = -3  /
&DEVC ID='WT3', XYZ= 0.25, -0.25, -0.01, QUANTITY='WALL TEMPERATURE', IOR = -3  /
&DEVC ID='WT4', XYZ= 0.25, 0.25, -0.01, QUANTITY='WALL TEMPERATURE', IOR = -3  /
&DEVC ID='WT5', XYZ= 0.00, 0.00, -0.01, QUANTITY='WALL TEMPERATURE', IOR = -3  /


&DEVC ID='WT6', XYZ= 0, 0.45, 0.01, QUANTITY='WALL TEMPERATURE', IOR = 3  /
&DEVC ID='WT7', XYZ= 0, 0.35, 0.01, QUANTITY='WALL TEMPERATURE', IOR = 3  /
&DEVC ID='WT8', XYZ= 0, 0.25, 0.01, QUANTITY='WALL TEMPERATURE', IOR = 3  /
&DEVC ID='WT9', XYZ= 0, 0.15, 0.01, QUANTITY='WALL TEMPERATURE', IOR = 3  /
&DEVC ID='WT10', XYZ= 0, 0.05, 0.01, QUANTITY='WALL TEMPERATURE', IOR = 3  /
&DEVC ID='WT11', XYZ= 0, -0.05, 0.01, QUANTITY='WALL TEMPERATURE', IOR = 3  /
&DEVC ID='WT12', XYZ= 0, -0.15, 0.01, QUANTITY='WALL TEMPERATURE', IOR = 3  /
&DEVC ID='WT13', XYZ= 0, -0.25, 0.01, QUANTITY='WALL TEMPERATURE', IOR = 3  /
&DEVC ID='WT14', XYZ= 0, -0.35, 0.01, QUANTITY='WALL TEMPERATURE', IOR = 3  /
&DEVC ID='WT15', XYZ= 0, -0.45, 0.01, QUANTITY='WALL TEMPERATURE', IOR = 3  /
&DEVC ID='WT16', XYZ= -0.45, 0, 0.01, QUANTITY='WALL TEMPERATURE', IOR = 3  /
&DEVC ID='WT17', XYZ= -0.35, 0, 0.01, QUANTITY='WALL TEMPERATURE', IOR = 3  /
&DEVC ID='WT18', XYZ= -0.25, 0, 0.01, QUANTITY='WALL TEMPERATURE', IOR = 3  /
&DEVC ID='WT19', XYZ= -0.15, 0, 0.01, QUANTITY='WALL TEMPERATURE', IOR = 3  /
&DEVC ID='WT20', XYZ= -0.05, 0, 0.01, QUANTITY='WALL TEMPERATURE', IOR = 3  /
```

```
&DEVC ID='WTRADPANELSBOTTOM', XYZ= 0, 0, -0.23, QUANTITY='WALL TEMPERATURE', IOR = -3 /
&DEVC ID='WTRADPANELTOP', XYZ= 0, 0, -0.21, QUANTITY='WALL TEMPERATURE', IOR = 3 /
////////////////////// Devices heat flux //////////////////////

&DEVC ID='rhfHeatedSide', XYZ= 0, 0, -0.01, QUANTITY='RADIATIVE HEAT FLUX', IOR = -3 /
&DEVC ID='rhfCooledSide', XYZ= 0, 0, 0.01, QUANTITY='RADIATIVE HEAT FLUX', IOR = 3 /
&DEVC ID='chfHeatedSide', XYZ= 0, 0, -0.01, QUANTITY='CONVECTIVE HEAT FLUX', IOR = -3 /
&DEVC ID='chfCooledSide', XYZ= 0, 0, 0.01, QUANTITY='CONVECTIVE HEAT FLUX', IOR = 3 /
&DEVC ID='thfHeatedSide', XYZ= 0, 0, -0.01, QUANTITY='TOTAL HEAT FLUX', IOR = -3 /
&DEVC ID='thfCooledSide', XYZ= 0, 0, 0.01, QUANTITY='TOTAL HEAT FLUX', IOR = 3 /

&DEVC ID='rhfRadPanelSide', XYZ= 0, 0, -0.21, QUANTITY='RADIATIVE HEAT FLUX', IOR = 3 /
&DEVC ID='chfRadPanelSide', XYZ= 0, 0, -0.21, QUANTITY='CONVECTIVE HEAT FLUX', IOR = 3 /
&DEVC ID='thfRadPanelSide', XYZ= 0, 0, -0.21, QUANTITY='TOTAL HEAT FLUX', IOR = 3 /

////////////////////// Boundary files //////////////////////

&BNDF QUANTITY='RADIATIVE HEAT FLUX'/
&BNDF QUANTITY='CONVECTIVE HEAT FLUX'/
&BNDF QUANTITY='TOTAL HEAT FLUX'/
&BNDF QUANTITY='NET HEAT FLUX'/
&BNDF QUANTITY='WALL TEMPERATURE'/

////////////////////// PDPA devices //////////////////////

//////////////// first PDPA focuses on the diameter histogram ////////////////

&PROP ID='pdpa_D',
PART_ID = 'Watermist',
QUANTITY = 'DIAMETER',
HISTOGRAM_CUMULATIVE = T,
PDPA_RADIUS = 0.01,
PDPA_START = 460.0,
PDPA_END = 560.0,
PDPA_M = 1,
HISTOGRAM =T,
HISTOGRAM_NBINS = 20,
HISTOGRAM_LIMITS = 0, 0.0004/

&DEVC XYZ= 0.00,0.0,0.02, QUANTITY='PDPA', PROP_ID='pdpa_D', ID='D1-0' /
&DEVC XYZ= 0.01,0.0,0.02, QUANTITY='PDPA', PROP_ID='pdpa_D', ID='D1-10' /
&DEVC XYZ= 0.02,0.0,0.02, QUANTITY='PDPA', PROP_ID='pdpa_D', ID='D1-20' /
```

```
&DEVC XYZ= 0.03,0.0,0.02, QUANTITY='PDPA', PROP_ID='pdpa_D', ID='D1-30' /
&DEVC XYZ= 0.04,0.0,0.02, QUANTITY='PDPA', PROP_ID='pdpa_D', ID='D1-40' /
&DEVC XYZ= 0.05,0.0,0.02, QUANTITY='PDPA', PROP_ID='pdpa_D', ID='D1-50' /
&DEVC XYZ= 0.06,0.0,0.02, QUANTITY='PDPA', PROP_ID='pdpa_D', ID='D1-60' /
&DEVC XYZ= 0.07,0.0,0.02, QUANTITY='PDPA', PROP_ID='pdpa_D', ID='D1-70' /
&DEVC XYZ= 0.08,0.0,0.02, QUANTITY='PDPA', PROP_ID='pdpa_D', ID='D1-80' /
&DEVC XYZ= 0.09,0.0,0.02, QUANTITY='PDPA', PROP_ID='pdpa_D', ID='D1-90' /
&DEVC XYZ= 0.10,0.0,0.02, QUANTITY='PDPA', PROP_ID='pdpa_D', ID='D1-100' /
&DEVC XYZ= 0.11,0.0,0.02, QUANTITY='PDPA', PROP_ID='pdpa_D', ID='D1-110' /
&DEVC XYZ= 0.12,0.0,0.02, QUANTITY='PDPA', PROP_ID='pdpa_D', ID='D1-120' /
&DEVC XYZ= 0.13,0.0,0.02, QUANTITY='PDPA', PROP_ID='pdpa_D', ID='D1-130' /
&DEVC XYZ= 0.14,0.0,0.02, QUANTITY='PDPA', PROP_ID='pdpa_D', ID='D1-140' /
&DEVC XYZ= 0.15,0.0,0.02, QUANTITY='PDPA', PROP_ID='pdpa_D', ID='D1-150' /
&DEVC XYZ= 0.16,0.0,0.02, QUANTITY='PDPA', PROP_ID='pdpa_D', ID='D1-160' /
&DEVC XYZ= 0.17,0.0,0.02, QUANTITY='PDPA', PROP_ID='pdpa_D', ID='D1-170' /
&DEVC XYZ= 0.18,0.0,0.02, QUANTITY='PDPA', PROP_ID='pdpa_D', ID='D1-180' /
&DEVC XYZ= 0.19,0.0,0.02, QUANTITY='PDPA', PROP_ID='pdpa_D', ID='D1-190' /
&DEVC XYZ= 0.20,0.0,0.02, QUANTITY='PDPA', PROP_ID='pdpa_D', ID='D1-200' /

/////////////// second PDPA focuses on the velocity histogram ///////////////

&PROP ID='pdpa_vel',
PART_ID = 'Watermist',
QUANTITY = 'VELOCITY',
HISTOGRAM_CUMULATIVE = T,
PDPA_RADIUS = 0.01,
PDPA_START = 460.0,
PDPA_END = 560.0,
PDPA_M = 0,
PDPA_N = 0,
HISTOGRAM =.TRUE.,
HISTOGRAM_NBINS = 20,
HISTOGRAM_LIMITS = 0, 40/

&DEVC XYZ= 0.00,0.0,0.02, QUANTITY='PDPA', PROP_ID='pdpa_vel', ID='v1-0' /
&DEVC XYZ= 0.01,0.0,0.02, QUANTITY='PDPA', PROP_ID='pdpa_vel', ID='v1-10' /
&DEVC XYZ= 0.02,0.0,0.02, QUANTITY='PDPA', PROP_ID='pdpa_vel', ID='v1-20' /
&DEVC XYZ= 0.03,0.0,0.02, QUANTITY='PDPA', PROP_ID='pdpa_vel', ID='v1-30' /
&DEVC XYZ= 0.04,0.0,0.02, QUANTITY='PDPA', PROP_ID='pdpa_vel', ID='v1-40' /
&DEVC XYZ= 0.05,0.0,0.02, QUANTITY='PDPA', PROP_ID='pdpa_vel', ID='v1-50' /
&DEVC XYZ= 0.06,0.0,0.02, QUANTITY='PDPA', PROP_ID='pdpa_vel', ID='v1-60' /
&DEVC XYZ= 0.07,0.0,0.02, QUANTITY='PDPA', PROP_ID='pdpa_vel', ID='v1-70' /
&DEVC XYZ= 0.08,0.0,0.02, QUANTITY='PDPA', PROP_ID='pdpa_vel', ID='v1-80' /
&DEVC XYZ= 0.09,0.0,0.02, QUANTITY='PDPA', PROP_ID='pdpa_vel', ID='v1-90' /
```

```
&DEVC XYZ= 0.10,0.0,0.02, QUANTITY='PDPA', PROP_ID='pdpa_vel', ID='v1-100' /
&DEVC XYZ= 0.11,0.0,0.02, QUANTITY='PDPA', PROP_ID='pdpa_vel', ID='v1-110' /
&DEVC XYZ= 0.12,0.0,0.02, QUANTITY='PDPA', PROP_ID='pdpa_vel', ID='v1-120' /
&DEVC XYZ= 0.13,0.0,0.02, QUANTITY='PDPA', PROP_ID='pdpa_vel', ID='v1-130' /
&DEVC XYZ= 0.14,0.0,0.02, QUANTITY='PDPA', PROP_ID='pdpa_vel', ID='v1-140' /
&DEVC XYZ= 0.15,0.0,0.02, QUANTITY='PDPA', PROP_ID='pdpa_vel', ID='v1-150' /
&DEVC XYZ= 0.16,0.0,0.02, QUANTITY='PDPA', PROP_ID='pdpa_vel', ID='v1-160' /
&DEVC XYZ= 0.17,0.0,0.02, QUANTITY='PDPA', PROP_ID='pdpa_vel', ID='v1-170' /
&DEVC XYZ= 0.18,0.0,0.02, QUANTITY='PDPA', PROP_ID='pdpa_vel', ID='v1-180' /
&DEVC XYZ= 0.19,0.0,0.02, QUANTITY='PDPA', PROP_ID='pdpa_vel', ID='v1-190' /
&DEVC XYZ= 0.20,0.0,0.02, QUANTITY='PDPA', PROP_ID='pdpa_vel', ID='v1-200' /

/////////////////// third PDPA focuses on the downwards velocity w histogram ///////////////////

&PROP ID='pdpa_velw',
PART_ID = 'Watermist',
QUANTITY = 'W-VELOCITY',
HISTOGRAM_CUMULATIVE = T,
PDPA_RADIUS = 0.01,
PDPA_START = 460.0,
PDPA_END = 560.0,
PDPA_M = 0,
PDPA_N = 0,
HISTOGRAM =.TRUE.,
HISTOGRAM_NBINS = 20,
HISTOGRAM_LIMITS = -40, 0/

&DEVC XYZ= 0.00,0.0,0.02, QUANTITY='PDPA', PROP_ID='pdpa_velw', ID='vw1-0' /
&DEVC XYZ= 0.01,0.0,0.02, QUANTITY='PDPA', PROP_ID='pdpa_velw', ID='vw1-10' /
&DEVC XYZ= 0.02,0.0,0.02, QUANTITY='PDPA', PROP_ID='pdpa_velw', ID='vw1-20' /
&DEVC XYZ= 0.03,0.0,0.02, QUANTITY='PDPA', PROP_ID='pdpa_velw', ID='vw1-30' /
&DEVC XYZ= 0.04,0.0,0.02, QUANTITY='PDPA', PROP_ID='pdpa_velw', ID='vw1-40' /
&DEVC XYZ= 0.05,0.0,0.02, QUANTITY='PDPA', PROP_ID='pdpa_velw', ID='vw1-50' /
&DEVC XYZ= 0.06,0.0,0.02, QUANTITY='PDPA', PROP_ID='pdpa_velw', ID='vw1-60' /
&DEVC XYZ= 0.07,0.0,0.02, QUANTITY='PDPA', PROP_ID='pdpa_velw', ID='vw1-70' /
&DEVC XYZ= 0.08,0.0,0.02, QUANTITY='PDPA', PROP_ID='pdpa_velw', ID='vw1-80' /
&DEVC XYZ= 0.09,0.0,0.02, QUANTITY='PDPA', PROP_ID='pdpa_velw', ID='vw1-90' /
&DEVC XYZ= 0.10,0.0,0.02, QUANTITY='PDPA', PROP_ID='pdpa_velw', ID='vw1-100' /
&DEVC XYZ= 0.11,0.0,0.02, QUANTITY='PDPA', PROP_ID='pdpa_velw', ID='vw1-110' /
&DEVC XYZ= 0.12,0.0,0.02, QUANTITY='PDPA', PROP_ID='pdpa_velw', ID='vw1-120' /
&DEVC XYZ= 0.13,0.0,0.02, QUANTITY='PDPA', PROP_ID='pdpa_velw', ID='vw1-130' /
&DEVC XYZ= 0.14,0.0,0.02, QUANTITY='PDPA', PROP_ID='pdpa_velw', ID='vw1-140' /
&DEVC XYZ= 0.15,0.0,0.02, QUANTITY='PDPA', PROP_ID='pdpa_velw', ID='vw1-150' /
&DEVC XYZ= 0.16,0.0,0.02, QUANTITY='PDPA', PROP_ID='pdpa_velw', ID='vw1-160' /
```

```
&DEVC XYZ= 0.17,0.0,0.02, QUANTITY='PDPA', PROP_ID='pdpa_velw', ID='vw1-170' /
&DEVC XYZ= 0.18,0.0,0.02, QUANTITY='PDPA', PROP_ID='pdpa_velw', ID='vw1-180' /
&DEVC XYZ= 0.19,0.0,0.02, QUANTITY='PDPA', PROP_ID='pdpa_velw', ID='vw1-190' /
&DEVC XYZ= 0.20,0.0,0.02, QUANTITY='PDPA', PROP_ID='pdpa_velw', ID='vw1-200' /

//////////////// fourth PDPA focuses on the water mass flux histogram ////////////////

&PROP ID='pdpa_massflux',
PART_ID = 'Watermist',
QUANTITY = 'PARTICLE FLUX Z',
HISTOGRAM_CUMULATIVE = T,
PDPA_RADIUS = 0.01,
PDPA_START = 460.0,
PDPA_END = 560.0,
PDPA_M = 1,
HISTOGRAM =.TRUE.,
HISTOGRAM_NBINS = 20,
HISTOGRAM_LIMITS = -0.00001, -0.00000008/

&DEVC XYZ= 0.00,0.0,0.02, QUANTITY='PDPA', PROP_ID='pdpa_massflux', ID='mf1-0' /
&DEVC XYZ= 0.01,0.0,0.02, QUANTITY='PDPA', PROP_ID='pdpa_massflux', ID='mf1-10' /
&DEVC XYZ= 0.02,0.0,0.02, QUANTITY='PDPA', PROP_ID='pdpa_massflux', ID='mf1-20' /
&DEVC XYZ= 0.03,0.0,0.02, QUANTITY='PDPA', PROP_ID='pdpa_massflux', ID='mf1-30' /
&DEVC XYZ= 0.04,0.0,0.02, QUANTITY='PDPA', PROP_ID='pdpa_massflux', ID='mf1-40' /
&DEVC XYZ= 0.05,0.0,0.02, QUANTITY='PDPA', PROP_ID='pdpa_massflux', ID='mf1-50' /
&DEVC XYZ= 0.06,0.0,0.02, QUANTITY='PDPA', PROP_ID='pdpa_massflux', ID='mf1-60' /
&DEVC XYZ= 0.07,0.0,0.02, QUANTITY='PDPA', PROP_ID='pdpa_massflux', ID='mf1-70' /
&DEVC XYZ= 0.08,0.0,0.02, QUANTITY='PDPA', PROP_ID='pdpa_massflux', ID='mf1-80' /
&DEVC XYZ= 0.09,0.0,0.02, QUANTITY='PDPA', PROP_ID='pdpa_massflux', ID='mf1-90' /
&DEVC XYZ= 0.10,0.0,0.02, QUANTITY='PDPA', PROP_ID='pdpa_massflux', ID='mf1-100' /
&DEVC XYZ= 0.11,0.0,0.02, QUANTITY='PDPA', PROP_ID='pdpa_massflux', ID='mf1-110' /
&DEVC XYZ= 0.12,0.0,0.02, QUANTITY='PDPA', PROP_ID='pdpa_massflux', ID='mf1-120' /
&DEVC XYZ= 0.13,0.0,0.02, QUANTITY='PDPA', PROP_ID='pdpa_massflux', ID='mf1-130' /
&DEVC XYZ= 0.14,0.0,0.02, QUANTITY='PDPA', PROP_ID='pdpa_massflux', ID='mf1-140' /
&DEVC XYZ= 0.15,0.0,0.02, QUANTITY='PDPA', PROP_ID='pdpa_massflux', ID='mf1-150' /
&DEVC XYZ= 0.16,0.0,0.02, QUANTITY='PDPA', PROP_ID='pdpa_massflux', ID='mf1-160' /
&DEVC XYZ= 0.17,0.0,0.02, QUANTITY='PDPA', PROP_ID='pdpa_massflux', ID='mf1-170' /
&DEVC XYZ= 0.18,0.0,0.02, QUANTITY='PDPA', PROP_ID='pdpa_massflux', ID='mf1-180' /
&DEVC XYZ= 0.19,0.0,0.02, QUANTITY='PDPA', PROP_ID='pdpa_massflux', ID='mf1-190' /
&DEVC XYZ= 0.20,0.0,0.02, QUANTITY='PDPA', PROP_ID='pdpa_massflux', ID='mf1-200' /

//////////////// fifth PDPA focuses on the water mass flux ////////////////

&PROP ID='pdpa_massfluxnor',
```

```
PART_ID = 'Watermist',
QUANTITY = 'PARTICLE FLUX Z',
PDPA_RADIUS = 0.01,
PDPA_START = 460.0,
PDPA_END = 560.0,
PDPA_M = 1/

&DEVC XYZ= 0.00,0.0,0.02, QUANTITY='PDPA', PROP_ID='pdpa_massfluxnor', ID='mfn1-0' /
&DEVC XYZ= 0.01,0.0,0.02, QUANTITY='PDPA', PROP_ID='pdpa_massfluxnor', ID='mfn1-10' /
&DEVC XYZ= 0.02,0.0,0.02, QUANTITY='PDPA', PROP_ID='pdpa_massfluxnor', ID='mfn1-20' /
&DEVC XYZ= 0.03,0.0,0.02, QUANTITY='PDPA', PROP_ID='pdpa_massfluxnor', ID='mfn1-30' /
&DEVC XYZ= 0.04,0.0,0.02, QUANTITY='PDPA', PROP_ID='pdpa_massfluxnor', ID='mfn1-40' /
&DEVC XYZ= 0.05,0.0,0.02, QUANTITY='PDPA', PROP_ID='pdpa_massfluxnor', ID='mfn1-50' /
&DEVC XYZ= 0.06,0.0,0.02, QUANTITY='PDPA', PROP_ID='pdpa_massfluxnor', ID='mfn1-60' /
&DEVC XYZ= 0.07,0.0,0.02, QUANTITY='PDPA', PROP_ID='pdpa_massfluxnor', ID='mfn1-70' /
&DEVC XYZ= 0.08,0.0,0.02, QUANTITY='PDPA', PROP_ID='pdpa_massfluxnor', ID='mfn1-80' /
&DEVC XYZ= 0.09,0.0,0.02, QUANTITY='PDPA', PROP_ID='pdpa_massfluxnor', ID='mfn1-90' /
&DEVC XYZ= 0.10,0.0,0.02, QUANTITY='PDPA', PROP_ID='pdpa_massfluxnor', ID='mfn1-100' /
&DEVC XYZ= 0.11,0.0,0.02, QUANTITY='PDPA', PROP_ID='pdpa_massfluxnor', ID='mfn1-110' /
&DEVC XYZ= 0.12,0.0,0.02, QUANTITY='PDPA', PROP_ID='pdpa_massfluxnor', ID='mfn1-120' /
&DEVC XYZ= 0.13,0.0,0.02, QUANTITY='PDPA', PROP_ID='pdpa_massfluxnor', ID='mfn1-130' /
&DEVC XYZ= 0.14,0.0,0.02, QUANTITY='PDPA', PROP_ID='pdpa_massfluxnor', ID='mfn1-140' /
&DEVC XYZ= 0.15,0.0,0.02, QUANTITY='PDPA', PROP_ID='pdpa_massfluxnor', ID='mfn1-150' /
&DEVC XYZ= 0.16,0.0,0.02, QUANTITY='PDPA', PROP_ID='pdpa_massfluxnor', ID='mfn1-160' /
&DEVC XYZ= 0.17,0.0,0.02, QUANTITY='PDPA', PROP_ID='pdpa_massfluxnor', ID='mfn1-170' /
&DEVC XYZ= 0.18,0.0,0.02, QUANTITY='PDPA', PROP_ID='pdpa_massfluxnor', ID='mfn1-180' /
&DEVC XYZ= 0.19,0.0,0.02, QUANTITY='PDPA', PROP_ID='pdpa_massfluxnor', ID='mfn1-190' /
&DEVC XYZ= 0.20,0.0,0.02, QUANTITY='PDPA', PROP_ID='pdpa_massfluxnor', ID='mfn1-200' /

//////////////// sixt PDPA focuses on the sauter mean diameter ////////////////

&PROP ID='pdpa_d32',
PART_ID = 'Watermist',
PDPA_M=3,
PDPA_N=2,
PDPA_RADIUS = 0.01,
PDPA_START = 460.0,
PDPA_END = 560.0/

&DEVC XYZ= 0.00,0.0,0.02, QUANTITY='PDPA', PROP_ID='pdpa_d32', ID='D32-0' /
&DEVC XYZ= 0.01,0.0,0.02, QUANTITY='PDPA', PROP_ID='pdpa_d32', ID='D32-10' /
&DEVC XYZ= 0.02,0.0,0.02, QUANTITY='PDPA', PROP_ID='pdpa_d32', ID='D32-20' /
&DEVC XYZ= 0.03,0.0,0.02, QUANTITY='PDPA', PROP_ID='pdpa_d32', ID='D32-30' /
&DEVC XYZ= 0.04,0.0,0.02, QUANTITY='PDPA', PROP_ID='pdpa_d32', ID='D32-40' /
```

```
&DEVC XYZ= 0.05,0.0,0.02, QUANTITY='PDPA', PROP_ID='pdpa_d32', ID='D32-50' /
&DEVC XYZ= 0.06,0.0,0.02, QUANTITY='PDPA', PROP_ID='pdpa_d32', ID='D32-60' /
&DEVC XYZ= 0.07,0.0,0.02, QUANTITY='PDPA', PROP_ID='pdpa_d32', ID='D32-70' /
&DEVC XYZ= 0.08,0.0,0.02, QUANTITY='PDPA', PROP_ID='pdpa_d32', ID='D32-80' /
&DEVC XYZ= 0.09,0.0,0.02, QUANTITY='PDPA', PROP_ID='pdpa_d32', ID='D32-90' /
&DEVC XYZ= 0.10,0.0,0.02, QUANTITY='PDPA', PROP_ID='pdpa_d32', ID='D32-100' /
&DEVC XYZ= 0.11,0.0,0.02, QUANTITY='PDPA', PROP_ID='pdpa_d32', ID='D32-110' /
&DEVC XYZ= 0.12,0.0,0.02, QUANTITY='PDPA', PROP_ID='pdpa_d32', ID='D32-120' /
&DEVC XYZ= 0.13,0.0,0.02, QUANTITY='PDPA', PROP_ID='pdpa_d32', ID='D32-130' /
&DEVC XYZ= 0.14,0.0,0.02, QUANTITY='PDPA', PROP_ID='pdpa_d32', ID='D32-140' /
&DEVC XYZ= 0.15,0.0,0.02, QUANTITY='PDPA', PROP_ID='pdpa_d32', ID='D32-150' /
&DEVC XYZ= 0.16,0.0,0.02, QUANTITY='PDPA', PROP_ID='pdpa_d32', ID='D32-160' /
&DEVC XYZ= 0.17,0.0,0.02, QUANTITY='PDPA', PROP_ID='pdpa_d32', ID='D32-170' /
&DEVC XYZ= 0.18,0.0,0.02, QUANTITY='PDPA', PROP_ID='pdpa_d32', ID='D32-180' /
&DEVC XYZ= 0.19,0.0,0.02, QUANTITY='PDPA', PROP_ID='pdpa_d32', ID='D32-190' /
&DEVC XYZ= 0.20,0.0,0.02, QUANTITY='PDPA', PROP_ID='pdpa_d32', ID='D32-200' /

//////////////// seventh PDPA focuses on the sauter mean diameter met diameter ////////////////

&PROP ID='pdpa_d32d',
PART_ID = 'Watermist',
QUANTITY = 'DIAMETER',
PDPA_M=3,
PDPA_N=2,
PDPA_RADIUS = 0.01,
PDPA_START = 460.0,
PDPA_END = 560.0/

&DEVC XYZ= 0.00,0.0,0.02, QUANTITY='PDPA', PROP_ID='pdpa_d32d', ID='D32d-0' /
&DEVC XYZ= 0.01,0.0,0.02, QUANTITY='PDPA', PROP_ID='pdpa_d32d', ID='D32d-10' /
&DEVC XYZ= 0.02,0.0,0.02, QUANTITY='PDPA', PROP_ID='pdpa_d32d', ID='D32d-20' /
&DEVC XYZ= 0.03,0.0,0.02, QUANTITY='PDPA', PROP_ID='pdpa_d32d', ID='D32d-30' /
&DEVC XYZ= 0.04,0.0,0.02, QUANTITY='PDPA', PROP_ID='pdpa_d32d', ID='D32d-40' /
&DEVC XYZ= 0.05,0.0,0.02, QUANTITY='PDPA', PROP_ID='pdpa_d32d', ID='D32d-50' /
&DEVC XYZ= 0.06,0.0,0.02, QUANTITY='PDPA', PROP_ID='pdpa_d32d', ID='D32d-60' /
&DEVC XYZ= 0.07,0.0,0.02, QUANTITY='PDPA', PROP_ID='pdpa_d32d', ID='D32d-70' /
&DEVC XYZ= 0.08,0.0,0.02, QUANTITY='PDPA', PROP_ID='pdpa_d32d', ID='D32d-80' /
&DEVC XYZ= 0.09,0.0,0.02, QUANTITY='PDPA', PROP_ID='pdpa_d32d', ID='D32d-90' /
&DEVC XYZ= 0.10,0.0,0.02, QUANTITY='PDPA', PROP_ID='pdpa_d32d', ID='D32d-100' /
&DEVC XYZ= 0.11,0.0,0.02, QUANTITY='PDPA', PROP_ID='pdpa_d32d', ID='D32d-110' /
&DEVC XYZ= 0.12,0.0,0.02, QUANTITY='PDPA', PROP_ID='pdpa_d32d', ID='D32d-120' /
&DEVC XYZ= 0.13,0.0,0.02, QUANTITY='PDPA', PROP_ID='pdpa_d32d', ID='D32d-130' /
&DEVC XYZ= 0.14,0.0,0.02, QUANTITY='PDPA', PROP_ID='pdpa_d32d', ID='D32d-140' /
&DEVC XYZ= 0.15,0.0,0.02, QUANTITY='PDPA', PROP_ID='pdpa_d32d', ID='D32d-150' /
```

```
&DEVC XYZ= 0.16,0.0,0.02, QUANTITY='PDPA', PROP_ID='pdpa_d32d', ID='D32d-160' /
&DEVC XYZ= 0.17,0.0,0.02, QUANTITY='PDPA', PROP_ID='pdpa_d32d', ID='D32d-170' /
&DEVC XYZ= 0.18,0.0,0.02, QUANTITY='PDPA', PROP_ID='pdpa_d32d', ID='D32d-180' /
&DEVC XYZ= 0.19,0.0,0.02, QUANTITY='PDPA', PROP_ID='pdpa_d32d', ID='D32d-190' /
&DEVC XYZ= 0.20,0.0,0.02, QUANTITY='PDPA', PROP_ID='pdpa_d32d', ID='D32d-200' /

/////////////////// eight PDPA focuses on the number concentration ///////////////////

&PROP ID='pdpa_NC',
PART_ID = 'Watermist',
QUANTITY = 'NUMBER CONCENTRATION',
PDPA_RADIUS = 0.01,
PDPA_START = 460.0,
PDPA_END = 560.0/

&DEVC XYZ= 0.00,0.0,0.02, QUANTITY='PDPA', PROP_ID='pdpa_NC', ID='NC1-0' /
&DEVC XYZ= 0.01,0.0,0.02, QUANTITY='PDPA', PROP_ID='pdpa_NC', ID='NC1-10' /
&DEVC XYZ= 0.02,0.0,0.02, QUANTITY='PDPA', PROP_ID='pdpa_NC', ID='NC1-20' /
&DEVC XYZ= 0.03,0.0,0.02, QUANTITY='PDPA', PROP_ID='pdpa_NC', ID='NC1-30' /
&DEVC XYZ= 0.04,0.0,0.02, QUANTITY='PDPA', PROP_ID='pdpa_NC', ID='NC1-40' /
&DEVC XYZ= 0.05,0.0,0.02, QUANTITY='PDPA', PROP_ID='pdpa_NC', ID='NC1-50' /
&DEVC XYZ= 0.06,0.0,0.02, QUANTITY='PDPA', PROP_ID='pdpa_NC', ID='NC1-60' /
&DEVC XYZ= 0.07,0.0,0.02, QUANTITY='PDPA', PROP_ID='pdpa_NC', ID='NC1-70' /
&DEVC XYZ= 0.08,0.0,0.02, QUANTITY='PDPA', PROP_ID='pdpa_NC', ID='NC1-80' /
&DEVC XYZ= 0.09,0.0,0.02, QUANTITY='PDPA', PROP_ID='pdpa_NC', ID='NC1-90' /
&DEVC XYZ= 0.10,0.0,0.02, QUANTITY='PDPA', PROP_ID='pdpa_NC', ID='NC1-100' /
&DEVC XYZ= 0.11,0.0,0.02, QUANTITY='PDPA', PROP_ID='pdpa_NC', ID='NC1-110' /
&DEVC XYZ= 0.12,0.0,0.02, QUANTITY='PDPA', PROP_ID='pdpa_NC', ID='NC1-120' /
&DEVC XYZ= 0.13,0.0,0.02, QUANTITY='PDPA', PROP_ID='pdpa_NC', ID='NC1-130' /
&DEVC XYZ= 0.14,0.0,0.02, QUANTITY='PDPA', PROP_ID='pdpa_NC', ID='NC1-140' /
&DEVC XYZ= 0.15,0.0,0.02, QUANTITY='PDPA', PROP_ID='pdpa_NC', ID='NC1-150' /
&DEVC XYZ= 0.16,0.0,0.02, QUANTITY='PDPA', PROP_ID='pdpa_NC', ID='NC1-160' /
&DEVC XYZ= 0.17,0.0,0.02, QUANTITY='PDPA', PROP_ID='pdpa_NC', ID='NC1-170' /
&DEVC XYZ= 0.18,0.0,0.02, QUANTITY='PDPA', PROP_ID='pdpa_NC', ID='NC1-180' /
&DEVC XYZ= 0.19,0.0,0.02, QUANTITY='PDPA', PROP_ID='pdpa_NC', ID='NC1-190' /
&DEVC XYZ= 0.20,0.0,0.02, QUANTITY='PDPA', PROP_ID='pdpa_NC', ID='NC1-200' /

&TAIL /
```

Appendix B

Extra results sensitivity radiation angles analysis

(a) RA 50
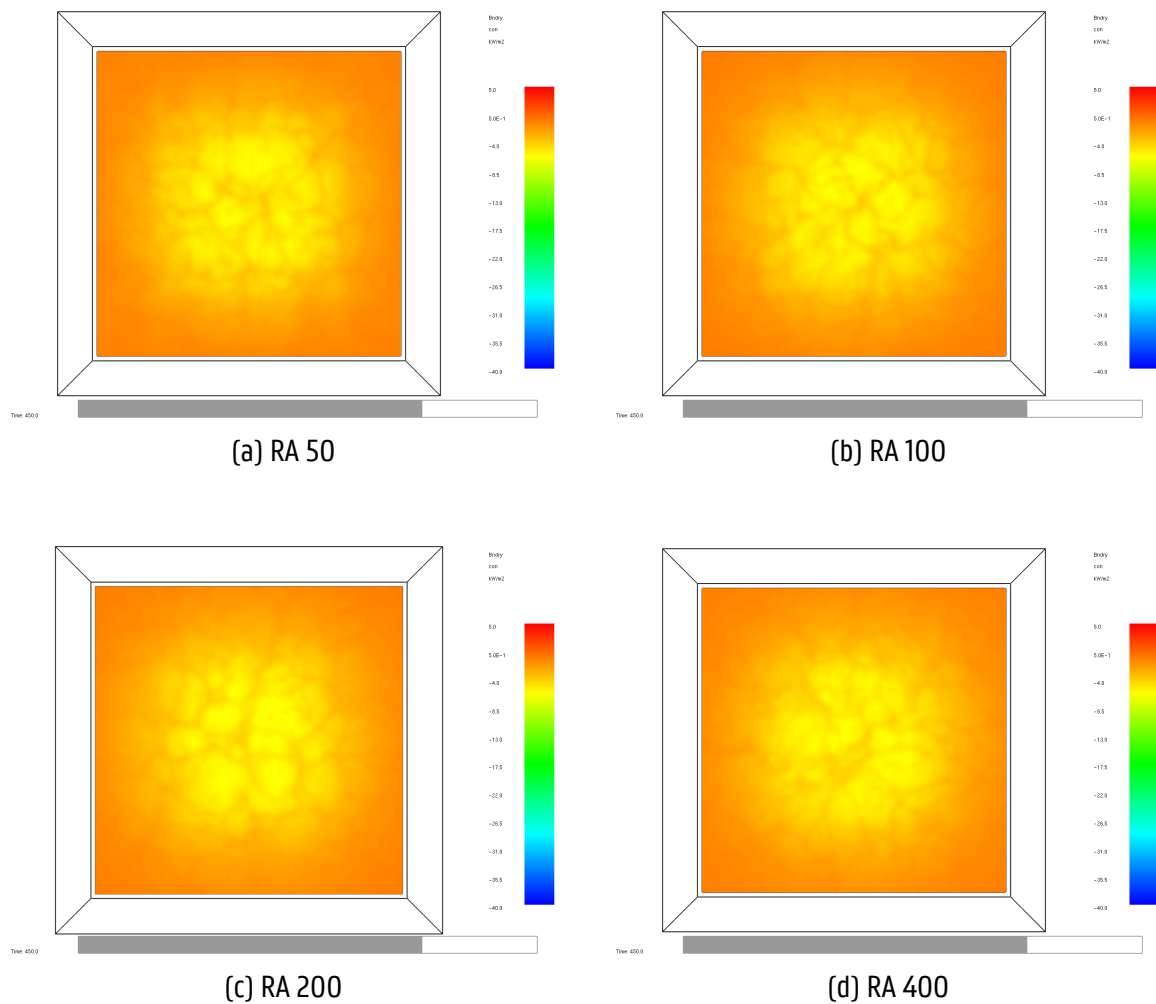
(b) RA 100

(c) RA 200

(d) RA 400

Figure 1: Convective Heat flux, Top view, Cool side, at 450 seconds with different number of radiation angles
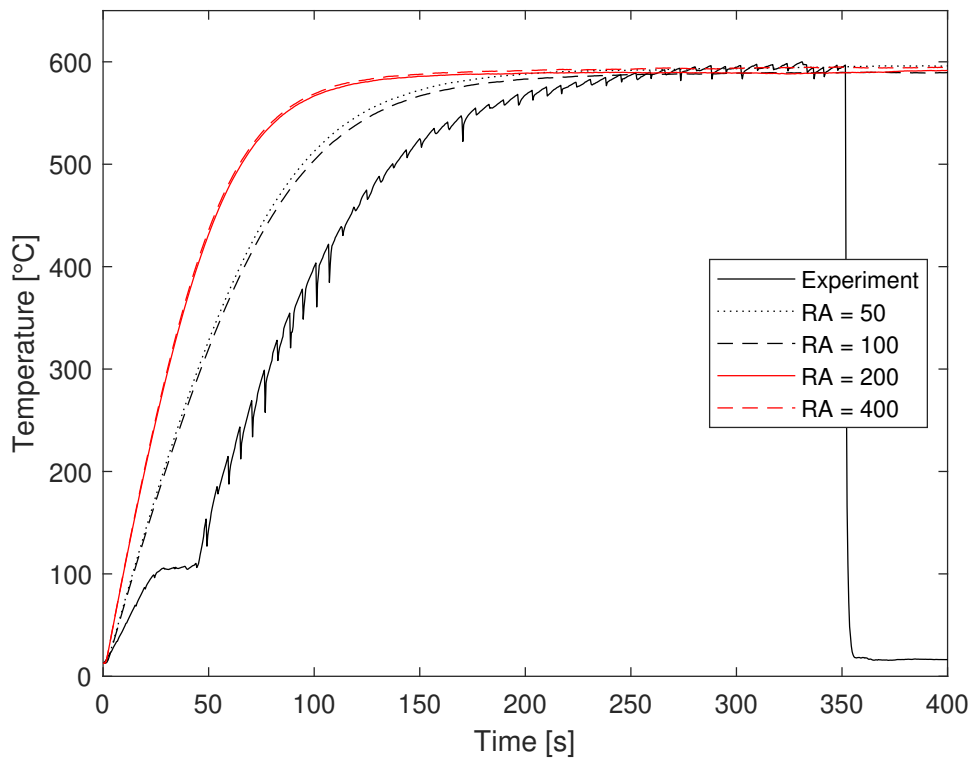
Figure 2: Wall temperature analysis steel plate with different RA values, Cool side

Appendix C

Size distribution

Matlab file

```matlab
clc
clear
close all
syms D
syms Y
syms X
gamma_D = 3.3
sigma_D = 1.15/gamma_D
D_median = 188 %Dv50
FuncDmedian = 400-D_median
ffirstpart = 1./(sigma_D*(sqrt(2.*pi)))

gamma_and_Dv50 = "Gamma= " + gamma_D + "  Dv50= "+ D_median

f = @(D) (0.5+((ffirstpart)*sqrt(pi/2.)*sigma_D*erf(((log(D)-log(
   D_median))/(sqrt(2)*sigma_D))))))

g = @(D) 1-exp(-0.693.*((D./D_median).^gamma_D))

for D = 1.0:D_median
    fplot(g, [0 D_median], 'red');
end

hold on

for Y = 1.0:FuncDmedian
    fplot(f, [D_median 400], 'red');
end

xlabel('Droplet size [microm]');
ylabel('Cumulative volume fraction of water');
```

```matlab
rawTable = readtable('MATLAB\dataCVF.xlsx','Sheet','Sheet1');

x = rawTable.Header1; %: get the excel column, Header1 (header name)
y = rawTable.Header2; %: get the excel column, Header2 (header name)

plot(x,y,'--','Color','black');

title('Rosin-Rammler distribution:', gamma_and_Dv50)

xlabel('Droplet size [microm]');
ylabel('Cumulative volume fraction of water');


qw{1} = plot(nan, '-','Color','red');
qw{2} = plot(nan, '--','Color','black');
legend([qw{:}], {'Simulation','Experiment'}, 'Location','northwest')

hold off
```
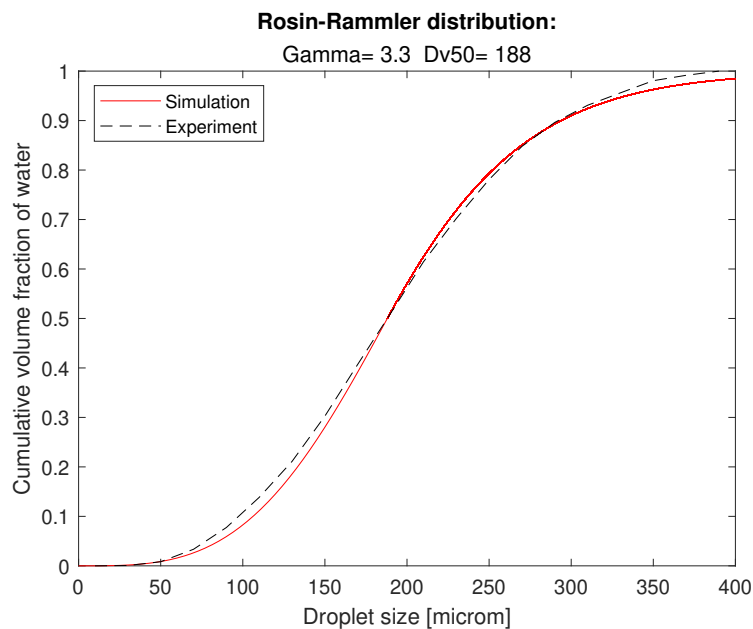
Graph size distribution

Figure 3: Graph Matlab of CVF Rosin-Rammler-log-normal distribution

Appendix D

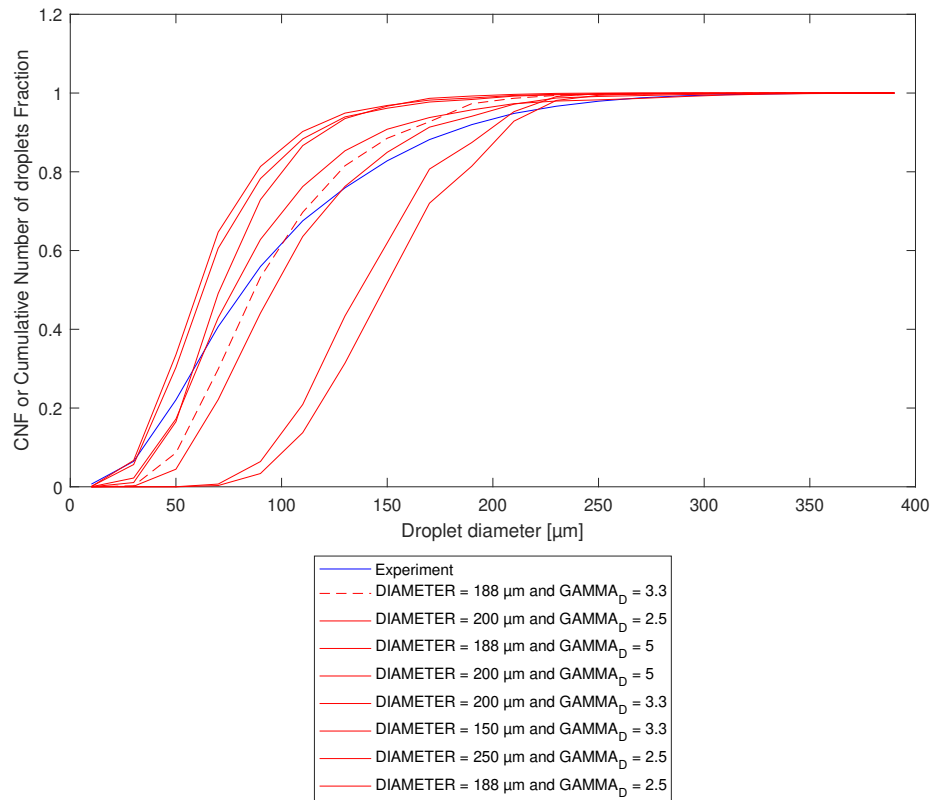## Different water spray distributions simulated

Size distributions

Figure 4: Multiple size distributions measured at 50 cm below the nozzle
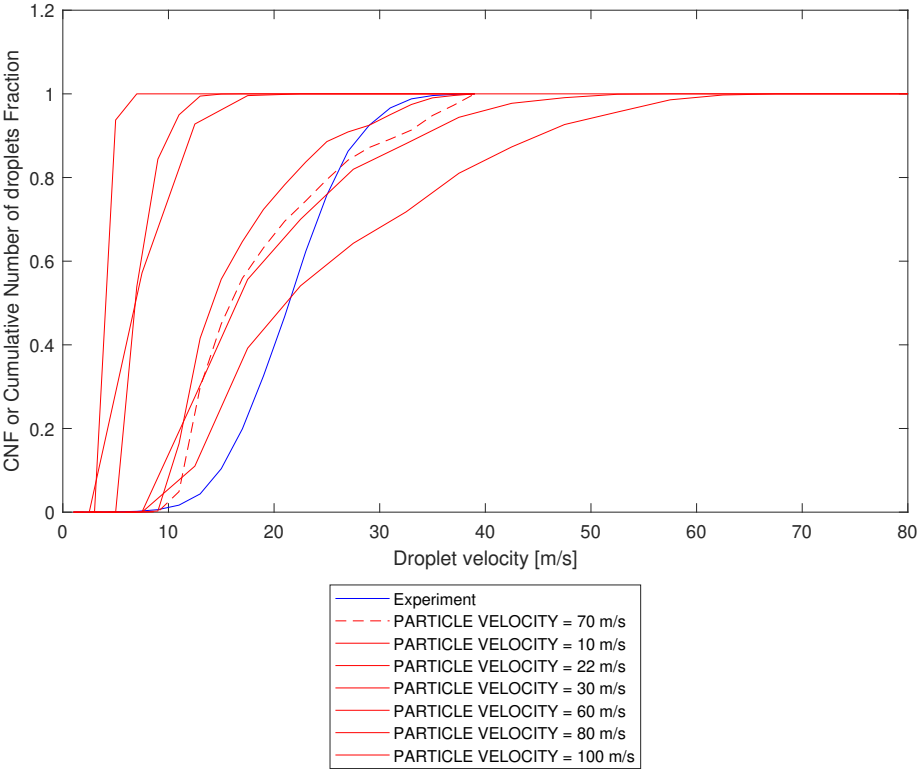
Velocity distributions

Figure 5: Multiple velocity distributions with different initial velocity out the nozzle measured at 50 cm below the nozzle